A COMPARATIVE STUDY BETWEEN ROTATIONAL AND VIRTUAL INERTIA: ROLE OF LIQUID AIR ENERGY STORAGE AS A SOURCE OF INERTIA IN FUTURE POWER SYSTEMS

Lappeenranta–Lahti University of Technology LUT

Master's Programme in Business Analytics, Master's thesis

2022

Pankaj O. Kela

Examiner(s): Professor Pasi Luukka

Professor Samuli Honkapuro

ABSTRACT

Lappeenranta–Lahti University of Technology LUT

LUT School of Engineering Science

Computational Engineering

Pankaj O. Kela

A COMPARATIVE STUDY BETWEEN ROTATIONAL AND VIRTUAL INERTIA: ROLE OF LIQUID AIR ENERGY STORAGE AS A SOURCE OF INERTIA IN FUTURE POWER SYSTEMS

Master's thesis

2022

76 pages, 38 figures, 18 tables and 0 appendices

Examiner(s): Professor Pasi Luukka and Professor Samuli Honkapuro

Keywords: Rotational Inertia, Virtual Inertia, Liquid Air Energy Storage, Power System Frequency Response.

Using power system frequency response simulations, this study develops understanding of the different factors that influence the capacity of fast energy storage systems and inverter capacity that can compensate for the reduction in synchronous rotational inertia. It is observed that the required virtual inertia (VI) capacity increases as the VI response time increases and, also with increases in the reference fault size. The required VI capacity also varies depending on the level of existing system inertia. The rate of increase in VI capacity increases as the system inertia decreases. This is also noted in the Nordic power system where the system inertia is at a high level and relatively small fast frequency response (FFR) capacity is suitable to sustain frequency nadir above desired limits. For example, at a particular simulation instant with relatively low inertia in the present Nordic grid, the FFR capacity of 62.4 MW suffices to improve the frequency nadir which would otherwise require almost 9.44 GWs of additional KE reserves. For the Cyprus power system, exploratory analysis looked at possible Liquid Air Energy Storage (LAES) scope and capacity to support a 100% renewable grid. Sources of synchronous rotational inertia (RI) such as LAES are believed to have a role in maintaining a minimum inertia base in the grid such that the RoCoF dynamics doesn't become prominent. If high amounts of RI are maintained in the system, then further gaps in inertia requirements can be addressed with limited capacity of fast energy storage. This study contributes towards a long-term view on the competitiveness of synchronous RI, considering the fast energy storage capacity and inverter capacity needed for VI.

ACKNOWLEDGEMENTS

This thesis work has been a milestone learning opportunity for me because it challenged and tested me in different ways. In many ways this journey has been a continuation of a previous one, and yet along the way situations came up that I was not prepared for. I am immensely grateful to everyone who has helped me undertake and complete this journey.

I am very thankful to my supervisor, Prof. Pasi Luukka, for his support and feedback at different stages of the work. Thank you also to my co-supervisor, Prof. Samuli Honkapuro, for the motivating discussions. Even before starting my Masters' studies, I was hoping to do my master's thesis on a topic combining analytics with applications in power sector. With the considerable challenges of inter-disciplinary research, I was not sure how it would happen. Your early encouragements to supervise me on the topic provided a big push in making this thought a reality.

A big thank you to my thesis guide and mentor at Sumitomo SHI FW, Pedro Giorni, for the extensive discussions in developing this work and the hands-on learning that I was fortunate to receive from him. His experience has greatly helped to give depth and breadth to this thesis work.

I also learned and benefited from the guidance and discussions with Edgardo Coda, Jeno Kovacs, Mikko Salo, Joona Heinonen, Jarno Nyman – thank you very much.

Special thanks to Mikko Kuivaniemi, from Fingrid, for the informative discussion, particularly in the context of the inertia related developments in the Nordic power system. One of the models implemented in this work is based on Mikko's research paper, which he kindly shared.

A warm thank you also to all my colleagues at Sumitomo SHI FW, interactions with whom made the daily work experience pleasant and joyful.

Thank you also to LUT University for making this journey possible in a supporting and cheerful environment.

Finally, I am very grateful to my family for their unflinching support and love. The support of family, present and future, is what keeps me going.

Abbreviations

AC	Alternating Current
DNO	Distribution Network Operator
DSO	Distribution System Operator
DGs	Distributed Generators
FCR	Frequency Containment Reserve
FFR	Fast Frequency Response
FRR	Frequency Restoration Reserve
IISW	Inverter Interfaced Solar and Wind
LAES	Liquid Air Energy Storage
MG	Microgrids
PLL	Phase Locked Loops
RI	Rotational Inertia
RoCoF	Rate of Change of Frequency
SG	Synchronous Generator
TSO	Transmission System Operator
UFLS	Under Frequency Load Shedding
VSG	Virtual Synchronous Generator
VI	Virtual Inertia

Contents

1. INTRODUCTION

This section gives an overview of the power system and its emerging concerns that motivates this master's thesis work. After an elaborate study of the research context, the research delimitations and objectives are identified.

1.1 Trend of Declining Power System Inertia

The evolution of the electrical power grid over the past century has been substantially shaped by one machine – the synchronous generator (SG). Whether the prime mover turning the rotor of the SG is powered by hydropower or nuclear power or by fossil fuels such as coal, oil, and gas, the Faraday laws of electromagnetic induction are at the heart of all these generators. Consequently, the power grid operations and dynamics are closely intertwined with the physical characteristics of SG.

The close link between power grid dynamics and SG characteristics will become more evident if we mentally switch-off for a moment the ubiquitous and extremely reliable electricity network of the present-day and rewind back a century to the early days electric power. Timo Myllyntaus, in his book, "The role of industry in the electrification of Finland", retraces the early days of adoption of electric power, *"from the introduction of the first permanent electric lighting plant in 1882 to the commission of the first nuclear plant in 1977"*. Of particular interest is to note that today's large, synchronous power grids emerged from distinct, independent small networks.

"The experience of Finland shows that it was geographically fairly small local networks which dominated the production and consumption of electricity up to World War II. For half a century, most of the electricity was consumed within the same industrial company or within the same small local network where it was generated. Consequently, the development of regional and national networks might not have had such an importance prior to 1940 as has been presumed. Although regional and national networks were commissioned in interwar-Finland, they gained a footing quite slowly. If this notion proves to be true in other countries as well, historians should pay more attention to these small networks and to self-generation instead of large technological systems

which became relevant only during and after World War II." [1]. Thus, the extensive electricity network has evolved from small local networks and SG machines operating for self-generation.

Indeed, the large electricity grid may be said to have coevolved interdependently with the electro-mechanical SG. Because SG has capability of reactive power provision that contributes to voltage stability and SG can operate self-organising, highly parallel, reliable and stable [2]. A particular SG characteristic that is de facto woven into supporting stable power grid operations is the mechanical rotational inertia of the rotating masses in a SG. Table 1 gives the inertia constant[1] values for the different SG plants.

Table 1. Values of the inertia constant [3]

Type of plant	**H (s)**
Nuclear	6 – 7
Coal and natural gas	3 – 6
Large Hydro	2 – 4
Small Hydro	1
Synchronous condenser	1

The inertia of all SGs in a particular grid collectively helps in enabling stable grid operations. Figure 1 shows the timescale of control actions in conventional power systems dominated by SG. The control actions escalate from Inertia Compensation to Primary Control to Secondary Control to Tertiary Control. Of significance here is SG's ability to resist changes in system frequency by Inertia Compensation (Figure 1) from the combined rotational inertia of all the heavy, spinning objects, termed system inertia. Inertia compensation offers an instantaneous response in the initial seconds of the frequency event, which gives a time window for activation of Primary Control. As per need, further control actions can be activated.

[1] Definition and explanation of Inertia constant is given in section 2.1

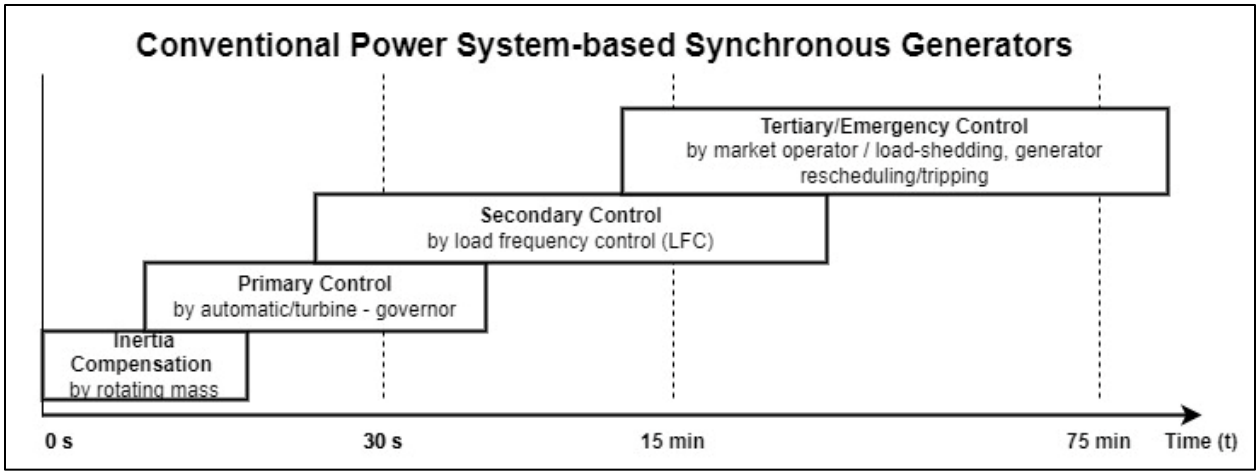

Figure 1. Frequency dynamics control timeline for synchronous generator-based power systems (reproduced from Figure 2.2 in [4])

However, there is now an ongoing transition from the centralised, fossil fuelled SG plants towards the more distributed, Solar and Wind Power plants. For example, Figure 2 illustrates this transition over two decades (1996 to 2016) in the generation mix in Europe. The proportion of renewable sources in Europe's generation mix increased from 14% in 1996 to 31% in 2016. This increase in renewable sources is contributed by Wind power, Solar Photovoltaic (PV) and Biomass + Biofuels.

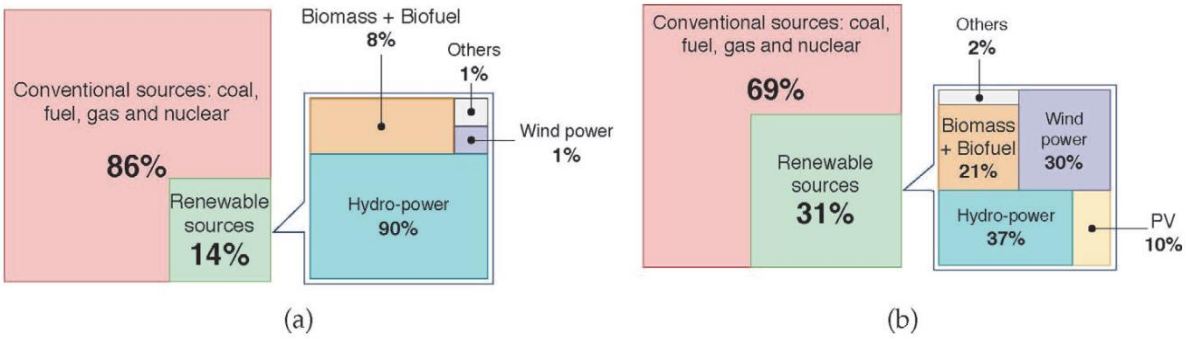

Figure 2. Generation mix in Europe: change between (a) 1996 and (b) 2016 (reproduced from Figure 5 in [5] under Creative Commons Attribution license)

These vital future energy sources of Wind and Solar PV are connected to the electricity grid through the power-electronic inverter interface [6]. Figure 3 shows a simple block diagram of the power-electronic inverter interface. This is a fundamentally distinct method of grid connection in

comparison to SG that are electro-mechanically coupled with the grid. As such, no inertia back-up is provided by the power-electronic interface to the grid.

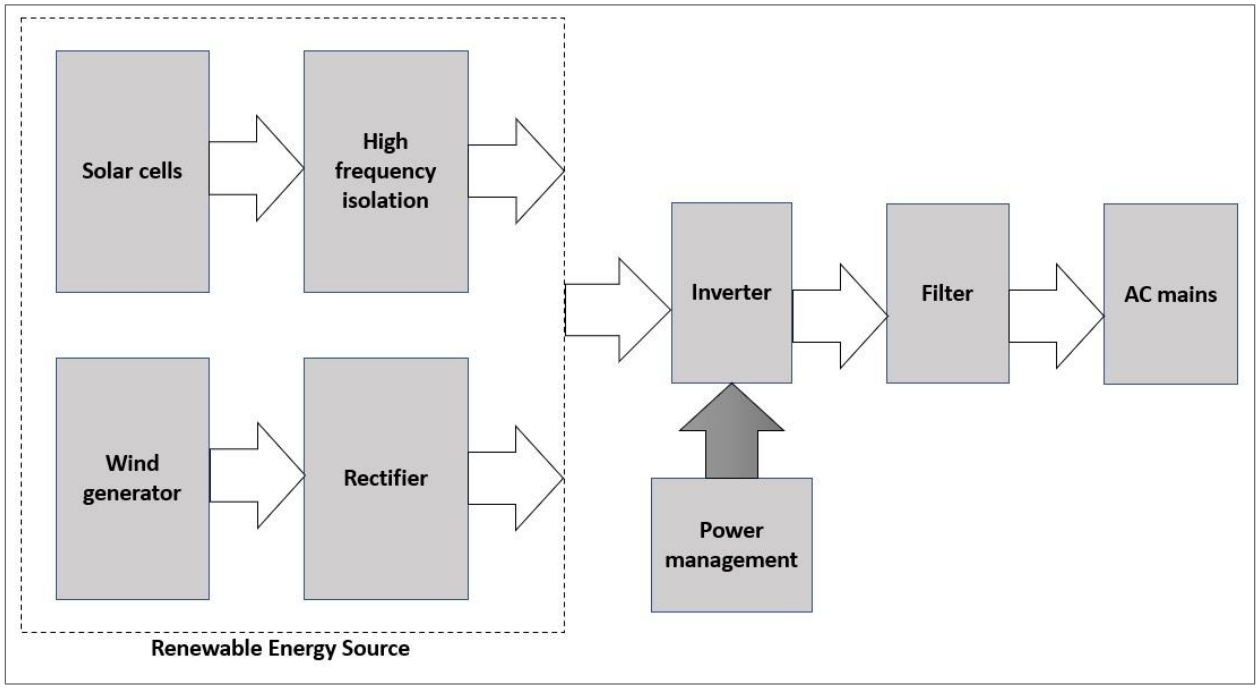

Figure 3. Block diagram of the power-electronic inverter interface of a renewable power system with the AC power grid (reproduced from Figure 1 in [7])

As these *inverter-interfaced Solar PV and Wind generators* (IISW) gain a stronger foothold in the generation mix of different regions, the rotating mass in the grid that can offer Inertia Compensation is declining. The result is declining trend of system inertia constants[2] as seen in Figure 4 for the different power grid regions in Europe and; a rise in the maximum frequency deviation [5], [2].

[2] System inertia constant is aggregate of individual generator inertia constants, defined in the Section 2.1

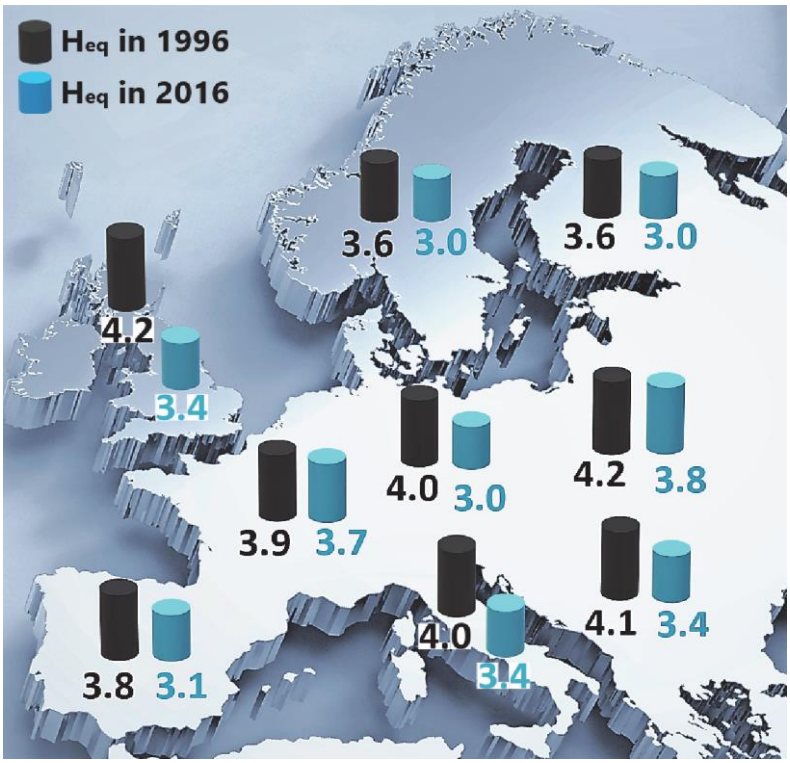

Figure 4. Change in Equivalent inertia constants estimated in EU-28 between 1996 and 2016 (reproduced from Figure 6 in [5] under Creative Commons Attribution license)

1.2 Impact of Declining System Inertia on the Frequency Response

The evolution from small local networks into ubiquitous and highly reliable national and regional electricity networks involves the co-ordinated response of the multiple generators to changes in demand. The generators supply power to the consumers through the transmission and distribution networks. Demand-supply co-ordination across these networks is made possible, among other aspects, by the system frequency of the interconnected alternating-current (AC) system. A characteristic of a synchronous AC grid, the overall grid shares a common standard electrical frequency (50 Hz/ 60 Hz). The mechanical rotor speed of SG and motor loads is coupled with the AC electrical frequency of the power grid by the electro-mechanical interface. The SG (and motor loads) spin at speeds proportional to system frequency.

Table 2 shows the frequency control standards provided by international grids. For different regions, the table gives the *nominal frequency*, the *normal operating frequency range*, and the *operational frequency tolerance range*.

i. When the system frequency is at nominal value (50 Hz/ 60 Hz), the supply from generators exactly meets the demand.
ii. The deviations within the *normal operating frequency range* may result from small changes in supply and demand and are acceptable.
iii. Any deviation outside the *normal operating frequency range* needs a control response to ensure that the system frequency is within the *operational frequency tolerance range*. As shown in Figure 1, the control actions are performed hierarchically in time. Particularly, inertia compensation gives some time to realise (or avoid) the activation of the primary control by slowing the rate of change in the frequency, and thus limiting the deviations.

Table 2: Frequency control standards provided by some international grids (Table 2.1 in [4], [8])

Country/ region	Japan	Australia	Europe	Great Britain	China	India
Nominal frequency	Eastern region: 50 Hz or Western region: 60 Hz	50 Hz	50 Hz	50 Hz	50 Hz	50 Hz
Normal operating frequency range	±0.2 Hz or ±0.3 Hz	Interconnected system: ±0.15 Hz Islanded system: ±0.5 Hz	±0.2 Hz	±0.5 Hz Target range: ±0.05 Hz	System ≥ 3 GW: ±0.2 Hz System< 3 GW: ±0.5 Hz	Target range: ±0.05 Hz
Operational frequency tolerance range	N/A	49-51 Hz Extreme frequency tolerance range: 47-52 Hz	49.2-50.8 Hz	49-51 Hz Under-frequency load shedding: 48.8 Hz	49-51 Hz	49.5–50.2 Hz

The large frequency deviations, outside the *normal operating frequency range*, typically result from a fault incident in the grid such as an unexpected generator failure. Figure 5 shows the frequency timeline before and after the fault incident. During steady state conditions, prior to the outage incident, minor variations in frequency are managed by automatic generation control. Next, the abrupt outage occurs and the frequency drops, initially declining at a rate inversely proportional

to system inertia[3]. The initial rate of change of frequency (RoCoF), the amount of frequency response provided, and the size of the generation trip determine the minimum frequency reached (the nadir) [9].

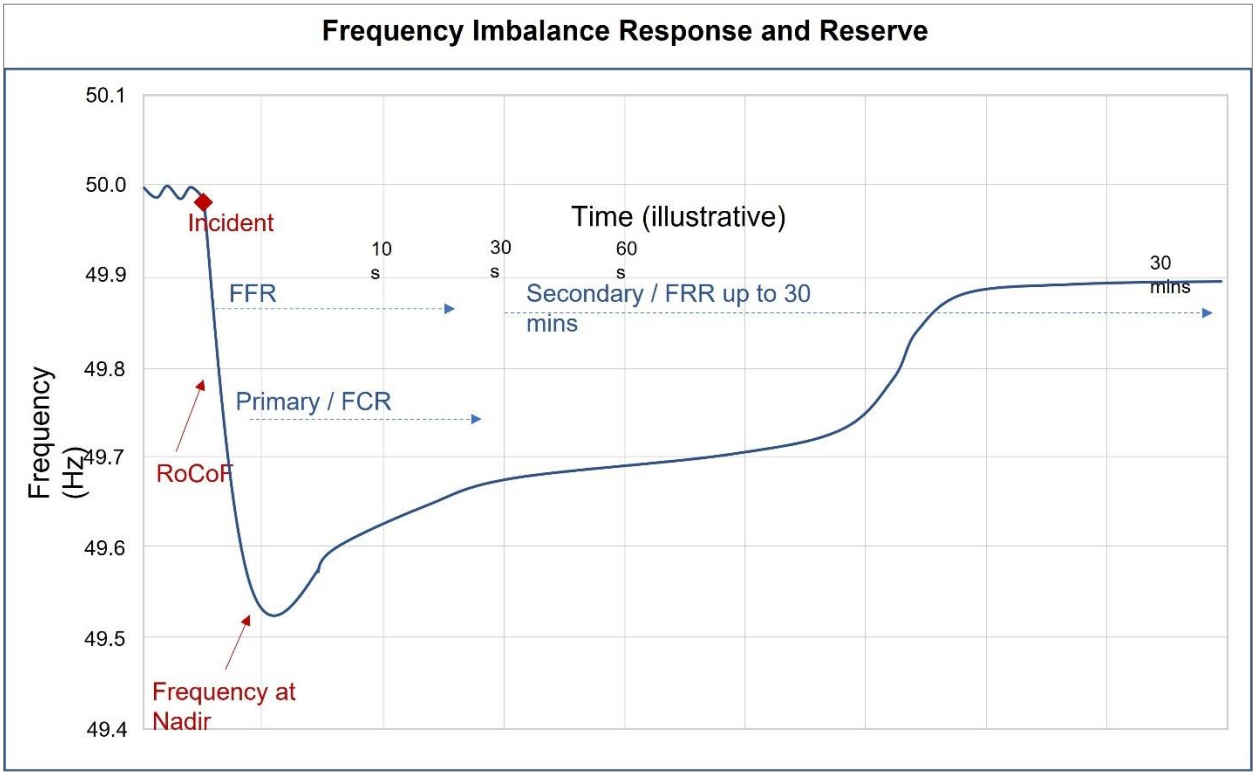

Figure 5. Graphical illustration of system frequency response over time, in case of a fault incident (reproduced from Figure 2 in [9])

Thus, the direct impact of low inertia is on the rate of change of frequency (RoCoF). Maintaining low RoCoF (< 0.5 Hz/s or <1 Hz/s) is significant to avoid potential instability in the power system. One potential high risk fault event that high RoCoF can cause is the loss of coupling of the electro-mechanically interfaced SG with the power grid, which can cascade into a full system blackout. Figure 6 shows the overall cause and effect of declining grid inertia [10], [11]. The decline in rotational inertia[4] is driving the RoCoF to increase, which impacts both the power system stability as well as operations. Thus, definitive actions are needed to mitigate the developing low system inertia.

[3] The inverse relation between system inertia and the rate of change of frequency (RoCoF) is derived in Section 2.1
[4] Rotational inertia, Grid inertia, System inertia, Kinetic inertia, Synchronous inertia, Mechanical inertia – these terms are used interchangeably, depending on the context/ source, to mean the available power system inertia.

--

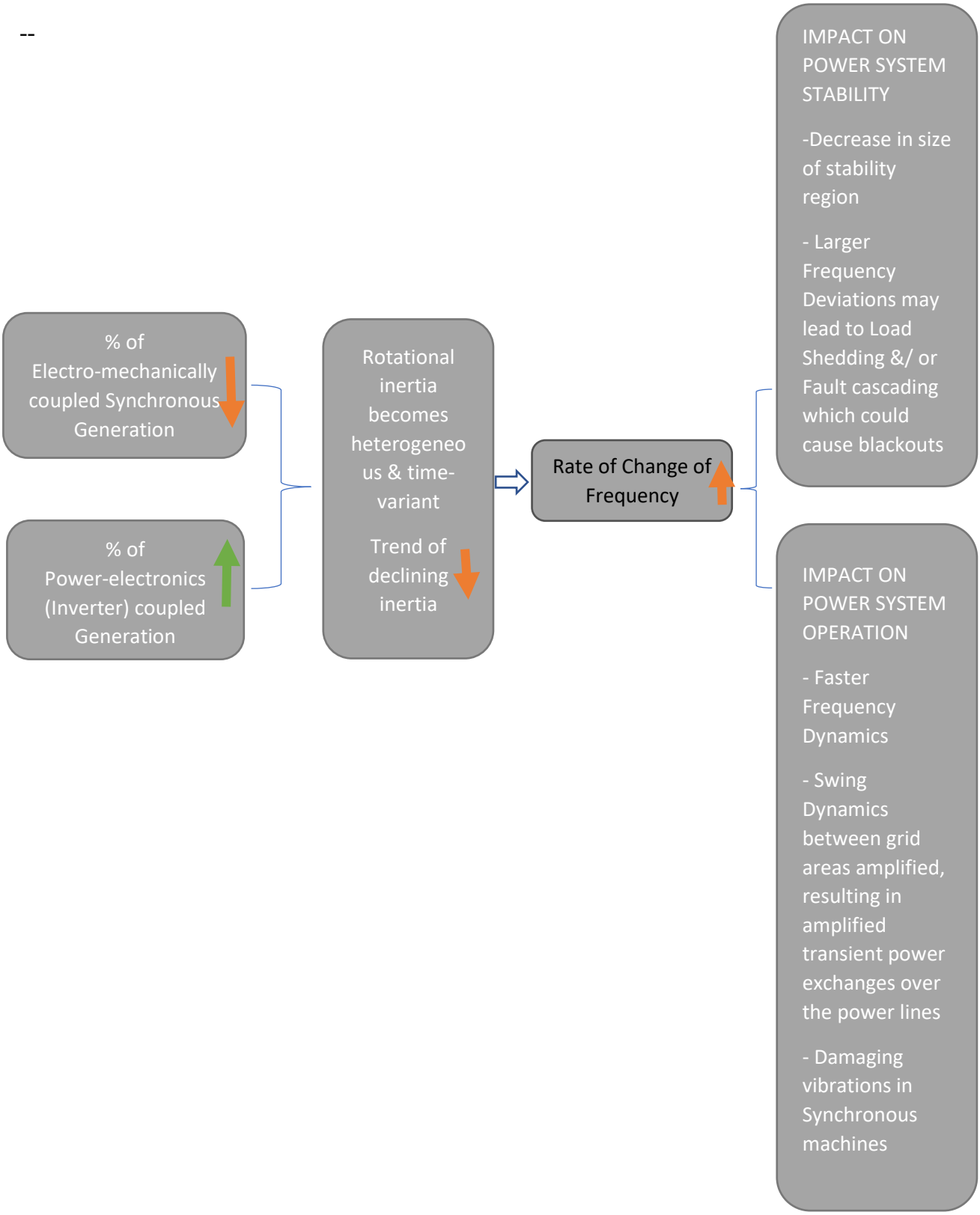

Figure 6. Visualising the cause and effect of declining rotational inertia in the power grid

1.3 Proposed options to mitigate the impact of low system inertia

In the previous sections, the reasons for decline in power system inertia and its impact on the stability and operations of the power grid have been described. The hitherto established approach of hierarchical control of deviations in grid-frequency (shown in Figure 1) to sustain stable and synchronous grid operations faces a shortfall in the very first stage of the control strategy – available *inertia compensation*. Although the increasing share of power-electronic interfaced renewable generators and the resulting issue of declining inertia is a common trend across international power grids [12], note from Table 2 that the different grids have different frequency standards. These differing standards point to the unique context and requirements of these power grids. None the less, three key characteristics of frequency in any synchronously interconnected power system are [3] –

i. Uniformity[5]: In power systems mainly based on mechanical inertia, the frequency is identical in every point and at any instant of the system because all the generators swing together, in synchronism.
ii. Coherency: A synchronized voltage waveform must be produced by the suitable correlation of all the generation units.
iii. Quasi-stability: Power system components are designed to operate optimally around the nominal frequency value (50 Hz / 60 Hz, see Table 2), and this mandates that the frequency must be maintained around this value. If the frequency deviation is greater than values that ensure safe operation (for example, outside the operational frequency tolerance range in Table 2), the protection systems built into the generating units disconnect the units from the power grid. Electrical loads are also designed for efficient operation at the nominal frequency value; productivity losses, equipment aging etc. results from recurrent deviations in frequency from the nominal value.

Now solutions are needed that maintain the status-quo of these system frequency characteristics. Two different approaches, with a comprehensive list of options proposed within each approach to mitigate impact of low system inertia on grid stability and operation are shown in Figure 7 [11], [13].

[5] The uniform frequency condition is not automatically valid in the ongoing situation with increasing inverter-interfaced generators replacing the classical SGs, and a new definition is needed [3]

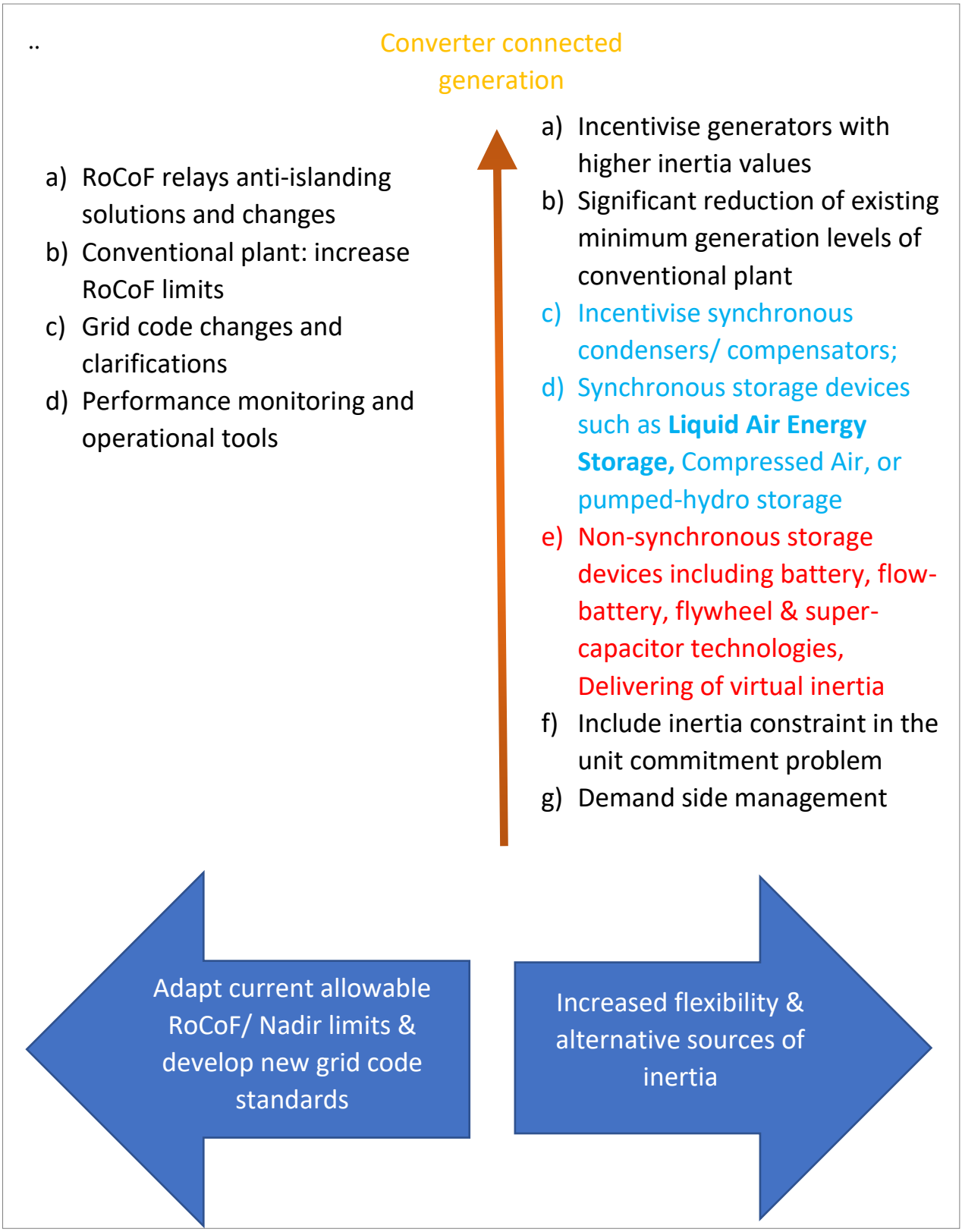

Figure 7. Different proposed options to operate a system with low synchronous inertia in a safe and secure way (adapted from Fig.11 in [11], [13])

The blue colour arrows in the bottom of Figure 7 are the two approaches, and the options within each approach are mentioned above them. The first approach is to *Adapt current allowable RoCoF/ Frequency Nadir limits and develop new grid codes* – this approach considers making changes or additions to the rules of the game, that is the performance criteria imposed by the grid on the different connecting assets. The second approach is to *Increase flexibility and alternative sources of inertia*. This approach considers new technologies, planning decisions and market design as the tools to increase the available system inertia. Thus, resources across the power system as well as diverse technology and market options are being explored and pooled together to manage and mitigate the impact of low power system inertia.

In the second approach, one technology path being considered is the use of Synchronous condensers [14] and Synchronous storage devices [13] (highlighted in blue colour in Figure 7) to increase the real Rotational Inertia (RI) in the grid, and thus increase the system inertia constant. Among the synchronous storage devices hitherto not considered for its potential to provide RI is the Liquid Air Energy Storage (LAES).

Another technology path being considered is the Virtual Inertia (VI) concept [15] (highlighted in red colour in Figure 7). VI refers to deploying fast responding, non-synchronous energy storage devices (also referred to as fast Energy Storage Systems or fast ESS) that inject active power in the grid, in a way that emulates the typical rotational inertia response. Non-synchronous, fast responding storage devices include battery storages, flow batteries, and super capacitor.

Thus, there is the possibility to augment system inertia constant with real RI provided by synchronous storage solutions such as LAES, and another possibility is to support the decline in system inertia constant by VI solutions that provide fast active power injection in the grid. Probably, both these possibilities will participate in supporting inertia needs of the future grid. None the less, how to compare these two alternatives, real RI and VI, with one another?

1.4 Research Motivation and Objectives

Along with the decline in power system inertia, a concomitant issue for the future power system is the escalating need for grid-scale (large scale) energy storages. Liquid Air Energy Storage (LAES), also referred to as Cryogenics-based energy storage, is the "*only energy storage technology so far, which is capable to store large quantities of electricity without geographical limitations or a substantive negative environmental impact*" [16]. The organization Sumitomo SHI FW has invested and partnered in the development of this novel technology. Some features of LAES are [17]-

i. Among Cryogenic Energy Storage medium, Air can be liquefied at around -195 ℃ and stored in insulated tanks. This technology is called Liquid Air Energy Storage.
ii. Energy produced by renewable sources at off-peak times is fed to an air liquefaction unit, while when electrical energy is needed, the liquid air could be pumped, heated and expanded into turbines to generate power.
iii. Compared to Pumped Hydro Storage and Compressed Air Energy Storage, LAES has significant energy density and is considered as a compact technology. Storage volume of LAES is reduced 6 times compared to CAES [18]. Also, unlike the former two storages, LAES also does not have geographical restrictions.
iv. LAES is currently at industrial demonstration level, and further development for commercial deployment are ongoing is ongoing.

In simple terms, LAES is equivalent to a combination of energy storage + synchronous condenser + flywheel. The synchronous condenser when connected to the grid in *'stability island'* mode has the capacity to provide inertia, as well as has added stabilizing effects on low inertia grid [14]. The LAES system inertia can be further significantly augmented by addition of a flywheel.

The challenges of low-inertia systems and need for grid-scale storages are largely being tackled independently – the diverging arrows in Figure 8a depict these independent directions in addressing the challenges faced by a common grid. Exploring synergies between the solutions for these two requirements, inertia and energy storage, could perhaps yield more economic and robust possibilities to fill the gaps in both these requirements – the converging arrows in Figure 8b depict the possibility of a common solution to the different challenges, questioning if LAES fits this role.

While LAES is developing in its prospective role as a grid-scale storage, of interest here is to understand the role LAES could play in supporting grid stability by providing additional rotational inertia. Thereby, improving its competitiveness.

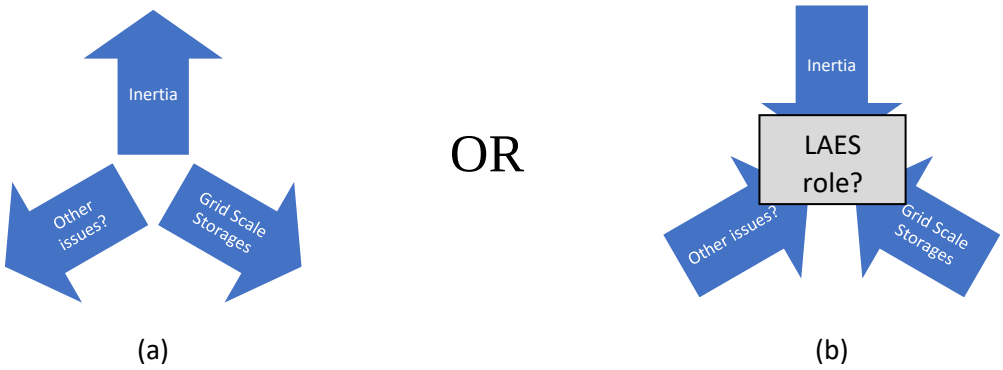

Figure 8. Finding convergence and synergy among the different challenges faced by the grid - does LAES fit this role (?)

In this background, the real RI that can be provided by LAES needs to be positioned with respect to the solutions that mimic inertia characteristics by way of fast active power injection, collectively referred to as virtual inertia (VI). Specifically, LAES as a source of synchronous 'real inertia' is to be evaluated in comparison to the non-synchronous fast ESS based VI solutions. This essentially translates into two questions-

- How to approach the choice between the real and virtual inertia? What are their relative technical/ commercial competences?
- What is the role of (or minimum requirement) of real inertia in the future grid?

To this end, the proposed approach is to estimate the fast response capacity that would be needed to steadily compensate for the decline in rotational inertia available in the grid. The idea here is to examine the size of increments needed in fast response capacity with declining grid inertia constant. This idea is visualised in Figure 9. The different lines in the Figure 9 indicate the different possible results. For example, if the result looks like either of the straight lines, this will imply that constant capacity increments are required for steady decrease in the grid's inertia state, proportional to the slope of the line (and independent of the depth of inertia decline). On the other hand, if the result looks like either of the two red colour curves, that will mean that the capacity

increments become larger as there is a deeper decline in grid inertia constant. Better understanding of this relationship will help to assess investments and future developments, when considering the choice between rotational or virtual inertia solution.

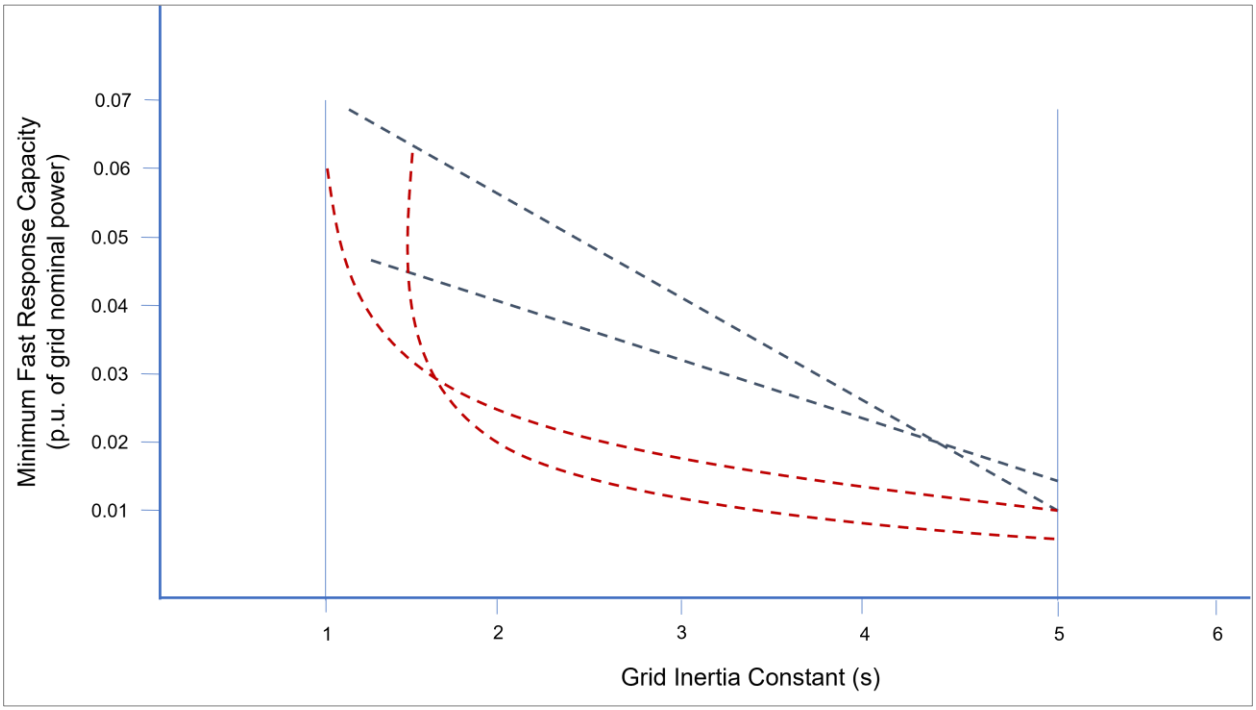

Figure 9. Symbolic visualization of results – each line indicates one possible result for the Minimum Fast Response Capacity (p.u.) in different levels of Grid Inertia Constant (s)

This thesis is interested in evolving a comparison between synchronous RI and non-synchronous VI, taking a long-term view of the low inertia trend. The research objectives of this thesis are:

A. For different level of grid inertia, what is the equivalent fast response capacity required to provide an inertia response that is like rotational inertia response?
B. Understand the different virtual inertia topologies and model a representative virtual inertia solution.
C. Understand, using models, the role of Liquid Air Energy Storage, as a source of rotational inertia to the grid.
D. Comprehend the results in specific grid scenarios.

Study Delimitations (factors that were controlled by the researcher):

- Power system parameters in the simulations (Chapter 4) were chosen by the researcher

Study Limitations (factors that were not under the control of the researcher):

- Even for very high volumes of power electronic renewable energy penetration being simulated, the power system is taken to have the structure of the synchronous frequency power system
- The model for virtual inertia is not selected or optimized considering the chosen power system parameters

Study Assumptions (factors that the researcher assumes were taken into consideration):

- Grid stability at very low inertia levels, that may be even below the *inertia floor*[6], was assumed in the simulations
- Simulation model assumes Primary Frequency Response is only sourced from the Synchronous Generators and there is no other source of Primary Frequency Response

[6] For inertia floor meaning, refer Table 6 in Chapter 3. Literature Review

2. THEORY

This section presents the theoretical background on the classical swing equation which is a well-known model representation for synchronous generators.

2.1 Power System Inertia Equation (Swing Equation) [10], [19]

The effect of the unbalance between the electromagnetic torque and the mechanical torque of the individual machines is described by the rotational inertia equations. These equations are of central importance in power system stability analysis.

The net torque causing acceleration (or deceleration), when there is an unbalance between the torques acting on the rotor is:

$$T_a = T_m - T_e \tag{1}$$

where
T_a = accelerating torque in N.m
T_m = mechanical torque in N.m
T_e = electromagnetic torque in N.m

T_m and T_e are positive for a generator and negative for a motor. The unbalance in the applied torque accelerates the combined inertia of the generator and the prime mover. Thus:

$$J\,\dot{\omega}_m = T_a = T_m - T_e \tag{2}$$

where
J = combined moment of inertia of generator and turbine, kg.m^2
$\dot{\omega}_m$ = time derivative of angular velocity (rotational speed) of the rotor, mechanical rad/s
t = time, s

Also,

$$\omega_m = 2\pi f_m \tag{3}$$

where
f_m = rotating frequency of the machine, Hz

Now, the rotational kinetic energy in the rotating masses of the generator system is given as:

$$E_{kin} = \frac{1}{2} J\,(2\pi f_m)^2 \tag{4}$$

where
E_{kin} = kinetic energy stored in the rotating masses of the generator system, watt-seconds, W.s

The inertia constant H for a synchronous machine is defined by:

$$H = \frac{stored\ energy\ at\ rated\ speed\ in\ MW.s}{rated\ power\ of\ the\ generator\ in\ MVA} \quad (5)$$

Thus:

$$H = \frac{E_{kin}}{S_B} = \frac{J\ (2\pi\ f_m)^2}{2\ S_B} \quad (6)$$

where
S_B = rated power of the generator, MVA
H = inertia constant, representing the combined inertia of the generator and the turbine, MW.s per MVA

The unit of H, *MegaWatt second per MegaVoltAmpere*, simplifies to seconds, *s*, and H denotes the time duration for which the machine's stored kinetic energy can supply its rated power. Typical values of H are in the range of 2 to 10 s, as shown in Table 3.

Table 3. Range of the inertia constant, H (reproduced from Table 3.2 in [19])

Type of synchronous generator	H (s)
Thermal unit (a) 3600 r/min (2-pole) (b) 1800 r/min (4-pole)	 2.5 to 6.0 4.0 to 10.0
Hydraulic unit	2.0 to 4.0

Thus, the higher the share of synchronous generators in the system, higher is the inertia constant H. Next, the inertial response of synchronous generator following a power imbalance can now be described in terms of the change in rotational frequency f_m (or rotational speed $\omega_m = 2\pi\ f_m$) of the synchronous generator:

$$\dot{E}_{kin} = J\ (2\pi)^2\ f_m\ .\ \dot{f}_m\ = \frac{2\ H\ S_B}{f_m}\ .\ \dot{f}_m\ =\ P_m - P_e \quad (7)$$

where
$\dot{E}_{kin}$ and $\dot{f}_m$ describes the time derivative E_{kin} and f_m
P_m = mechanical power supplied by the generator
P_e = electric power demand

Typically, the frequency excursions are small deviations around the reference value. So, f_m can be approximated with f_0 and P_m with $P_{m,0}$. With this background and, adding the frequency-dependent load damping, a self-stabilising property of power systems, the classical Swing Equation is completed:

$$\dot{f}_m = -\frac{f_0}{2\,H\,S_B D_{load}}\,f_m + \frac{f_0}{2\,H\,S_B}\,(P_{m,0} - P_e) \tag{8}$$

where
f_0 = reference frequency (typically 50 Hz or 60 Hz)
D_{load} = frequency-dependent load damping constant
$P_{m,0}$ = nominally scheduled mechanical generator power

Thus, for higher inertia constant H, the frequency dynamics for identical faults will be slower and more benign, that is frequency deviations, f_m, and their derivatives, $\dot{f}_m$, will be smaller. Note that $\dot{f}_m$ represents the Rate of Change of Frequency (RoCoF). The Aggregated Swing Equation (ASE) extends the model for individual generators to interconnected power systems. The ASE model supposes that the grid is highly meshed with all the units connected to the same grid bus, representing the Center of Inertia of the given grid. The classical Swing Equation (Eq. 8) is reformulated for a power system with n generators, j loads and l connecting tie-lines as:

$$\dot{f} = -\frac{f_0}{2\,H\,S_B D_{load}}\,f + \frac{f_0}{2\,H\,S_B}\,(P_m - P_{load} - P_{loss}) \tag{9}$$

where

$f = \frac{\sum_{i=1}^{n} H_i\, S_{B,i}\, f_i}{\sum_{i=1}^{n} H_i\, S_{B,i}}$ = the Center of Inertia grid frequency; f_0 = 50Hz / 60 Hz

$S_B = \sum_{i=1}^{n} S_{B,i}$ = the total rated power of the generators

$H = \frac{\sum_{i=1}^{n} H_i\, S_{B,i}}{S_B}$ = the aggregated inertia constant of the n generators

$P_m = \sum_{i=1}^{n} P_{m,i}$ = the total mechanical power of the generators

$P_{load} = \sum_{i=1}^{j} P_{load,i}$ = the total system load of the grid

$P_{loss} = \sum_{i=1}^{l} P_{loss,i}$ = the total transmission losses of the l lines making up the grid topology

D_{load} = frequency damping of the system load, is assumed here to be constant and uniform

3. LITERATURE REVIEW

In discussions and readings prior to the project, the general power system context and macro developments leading up to the research problem were understood. In context of grid inertia, there are a diversity of topics that consider different aspects of the problem. Given the voluminous literature on the subject, a more fine-tuned search process was needed to uncover the relevant research question/s considering the host organisation's context and requirements.

To begin with, the generic key phrase *"grid inertia frequency regulation"* was used to search the databases of *IEEE Xplore* and *Scopus* on 7th April 2021. From the search results, about 90 research papers that seemed relevant for the topic were selected. Then a manual clustering of the papers into groups was undertaken – papers that seemed to be considering similar research questions were grouped together. From this grouping six clusters of research topics/ questions in the context of grid inertia emerged. These six clusters are:

A. Impact of variable system inertia
B. Inertia estimation
C. Impact of inertia emulation on Protection
D. Inertia emulation methods, control mechanisms
E. Different sources of inertia such as energy storages, demand response
F. Low inertia trends and solutions across the globe

This clustering was used as a quick fix to aid in information management and classification. It is expected that the research papers would generally span across multiple clusters. To further narrow down among these six clusters, a comparative ranking of these clusters in terms of their importance for the research context was requested from the project mentor. This process helped to filter through the large volume of research papers, identify focus areas of the study and improve upon the articulation of the research problem. Table 4 shows the tentative relevance ranking given to the clusters.

Table 4: Relevance ranking of the research clusters

Topic	Impact of variable system inertia	Inertia estimation	Impact of inertia emulation on Protection	Inertia emulation methods, control mechanisms	Sources of inertia such as different energy storages, demand response	Low inertia trends and solutions across the globe
Rank	**V**	**IV**	**V**	**I**	**III**	**II**

Thus, the top three relevant clusters are:

i. Inertia emulation methods, control mechanisms
ii. Low inertia trends and solutions across the globe
iii. Sources of inertia

These clusters guided the initial literature study. As the research approach and objectives became more definitive, the focus was more towards studying literature that answered questions that emerged during the model and simulation development. A literature review of the key topics is presented next.

The analysis by Ulbig et al. ([10]) highlights that the traditional assumptions about power system inertia need to be reconsidered considering high shares of inverter-connected generation. Analysis is presented for up to three-area power systems using the Aggregated Swing Equation model, with the comment that "it is known that frequency dynamics for a system with n areas can become chaotic in case $n \geq 3$". Traditionally rotational inertia constant value has been assumed to be homogenous and time invariant in a power system. The paper demonstrates that-

- Rotational inertia (RI) does not remain a homogeneous power system property but becomes heterogeneous. That is, depending on the proportion of converter-connected units versus conventional units that are online in individual areas *i*, there are different H_i for these areas, instead of a global inertia constant H.
- Due to variability of the power dispatch, RI constant is also no longer stable in value over time but becomes time-variant ($H_i(t)$). Thus, individual grid areas also have variable rates of frequency dynamics.
- Frequency instability phenomena are amplified in the grid. Reduced RI causes faster frequency dynamics which, in the event of a power fault, leads to larger frequency

deviations and transient power exchanges over tie-lines. This can cause unexpected tripping of the tie-lines in question by automatic protection devices, in turn making a critical situation worse.

- Simulations demonstrate that time-variant damping effect (k(t)) is emulated by faster primary control, and the fast response behaviour of BESS units is aptly suited for providing either synthetic inertia or fast frequency (and voltage) control reserves for power system operation. [10]

While low inertia amplifies the frequency instability phenomena in the grid, there are also other factors to contend with when understanding the overall picture of frequency stability. Denholm et al. ([20]), in their lucid report describe the different factors that impact the frequency stability. Table 5 gives the list of factors and their relation in driving frequency stability.

Table 5: Summary of Factors that drive frequency stability (reproduced from Table 1 in [20])

Factor	**Impact of greater amount (assuming no other factors change)**
Generator inertia	Slows down frequency decline
Load inertia and load damping	Slows down frequency decline
Contingency size (reference fault size)	Increases frequency decline
Underfrequency limits (UFLS settings)	Lower UFLS settings provides more time for overall response
Frequency response speed	Responds faster to a decline in frequency

The detailed description of these factors is not reported here. After consideration of all the above factors, the required minimum inertia, that can ensure frequency stability in the power system, can be estimated. The report by Electric Power Research Institute [9] gives the values of these factors (constraints) for different power systems and also determines the inertia floor, that is the minimum required inertia in the grid for frequency stability. These values are reported in Table 6. Note in this table that the maximum allowed frequency deviation (UFLS stage 1) as well as the maximum allowed RoCoF is for the South Australian grid, with values of 47.6 Hz and 1.5 to 3 Hz/s respectively. This allowance for large and fast frequency deviations, along with lower values of contingency and peak demand result in the lowest value of inertia floor (6.2 GWs) for the South Australian grid. That is, if a grid allows for large and fast frequency deviations, it can get by with

lower values of system inertia[7]. The highest inertia floor requirements are for the Great Britain (National Grid) and the Nordic System, with values of 135 GWs and 125 GWs, respectively,

Table 6. Practical requirements for determining minimum inertia (reproduced from Table 2 in [9])

Constraint	Texas (ERCOT)	Great Britain (National Grid)	Ireland (EirGrid)	Nordic System	South Australia
UFLS stage 1	59.3 Hz	48.8 Hz	48.85 Hz	48.85 Hz	47.6 Hz
RoCoF	1 Hz/s	0.5 Hz/s	1 Hz/s	0.5 Hz/s	1.5 - 3 Hz/s
Contingency	2.75 GW	1.25 GW	0.5 GW	1.65 GW	0.35 GW
Peak demand	~73 GW	~60 GW	~6.5 GW	~72 GW	~3.4 GW
Inertia floor	100 GWs	135 GWs	23 GWs	125 GWs	6.2 GWs

Table 6 shows that the power systems significantly differ from each other in terms of the values of the different frequency stability factors and the required inertia floor. It was noted in Table 2 (section 1.2) that different power grids have different ranges in which they determine the normal and operational frequency. This table shows that the defined frequency ranges happen in conjunction with factors related to the grid engineering such as Under-frequency Load Shedding, contingency and peak demand. Also, the initial thought at the start of the thesis project posited a generic comparison between rotational and virtual inertia. This table explains the need for defined grid context and specificity, for a meaningful comparison of alternative inertia solutions, as the inertia levels to be maintained in the different grids are different. Further differences are noted in Table 7, which shows the different power grids are guided by differing priorities between RoCoF and Frequency Nadir to determine the minimum inertia levels.

Table 7. Criteria for determining minimum inertia levels of different system operators [4]

System operator	RoCoF	Frequency nadir
EirGrid (Ireland)	✓	
National Grid (UK)	✓	
AEMO (Australia)	✓	✓
ERCOT (Texas, USA)		✓
NORDIC (Scandinavia)		✓

[7] This is an example of what is being referred in the Figure 7 in section 1.3 regarding adapting the RoCoF and frequency Nadir values to accommodate low system inertia.

The context of inertia requirement and its relationship with grid frequency is now well understood. Next, the need is to learn the different approaches pursued to mitigate low system inertia. A comprehensive list of approaches is given in Figure 7 (section 1.3). That list is however missing one category of approach, that is non-synchronous fast frequency reserves (non-synchronous energy storges, that is mentioned in Figure 7, is a subset of this category).

Karbouj et al. ([21]) presents a literature review from the research and industry communities on possible sources of non-synchronous fast frequency reserve. The comprehensive list of the different possible non-synchronous fast frequency response reserves is shown in Table 8.

Table 8. Summary of non-synchronous fast frequency response reserves (reproduced from [21])

Resource	**Technique**	**Response type**	**Response time**	**Response duration**	**Volume**	**Extra infrastructure requirement[a]**	**Sub-optimum operation**
Wind power generation	overproduction	+	fast	limited by cut-in speed	Low	negligible	No
	deloading	+	moderate	throughout the operating period	Depends on headroom	negligible	yes
PV power plant	emulation from DC link	+	fast	Limited by minimum allowed DC link voltage	Very low	negligible	No
	Deloading	+	fast	throughout the operating period	Depends of headroom	negligible	yes
ESS	distributed ESS	+/-	fast	limited by ESS capacity	low	Yes	No
	Wind/Solar augmented ESS	+/-	fast	Limited by ESS power & wind/solar headroom	Limited by ESS power & wind/solar headroom	yes	Yes if wind/solar is deloaded
HVDC	emulation from DC link	+	fast	Limited by minimum allowed DC link voltage	Low	negligible	No
	HVDC connected wind farms	+	moderate	Depends on wind farm control technique	Depends on wind farm control technique	negligible	Yes if wind farm is deloaded
Demand response	passive	-	fast	Limited by owner's comfort	Depends on contracted demand	negligible	No
	active	+/-	fast	Limited by owner's comfort	Positive response is limited by ESS capacity	yes	no

[a] Extra infrastructure refers to the additional resource infrastructure that is required to enable FFR service from the source. For example, a new dedicated DESS may need to be installed to provide FFR service to the system, hence installing such devices will result in additional cost, which is not the case in modifying existing resources such as wind and solar power plants.

From these different possible non-synchronous fast frequency reserves, the virtual inertia from fast ESS is now described in detail. When comparing rotational and virtual inertia, rotational inertia is well understood and modeled. VI concept, on the other hand, is under development and it has spawned multiple designs, nomenclatures, and topologies. The nomenclature for VI concept

differs among different papers. As the driving motivation of the current work is to bring forth a comparative evaluation between rotational and virtual inertia, the diversity of nomenclatures and technical nuances that fall within the overarching VI concept are not delved upon in detail. Instead, the diverse nomenclatures and designs are all seen collectively as being a 'virtual' alternative to real/ rotational inertia. With this understanding, the VI concept is referred to by the name used in the respective paper being reviewed and additional definition/ clarification is attached to the name if the context requires it.

Bevrani et al. ([22]) reviews the main concept of Virtual Synchronous Generator (VSG), their role to support power grid control and presents a survey of the important VSG topologies. As shown in Figure 10, the VSG concept involves using appropriate control mechanism for short term (and fast-acting) energy storage together with a power electronics inverter/ converter, to establish virtual inertia for distributed generators (DGs) or renewable energy sources (RESs).

a)

b)

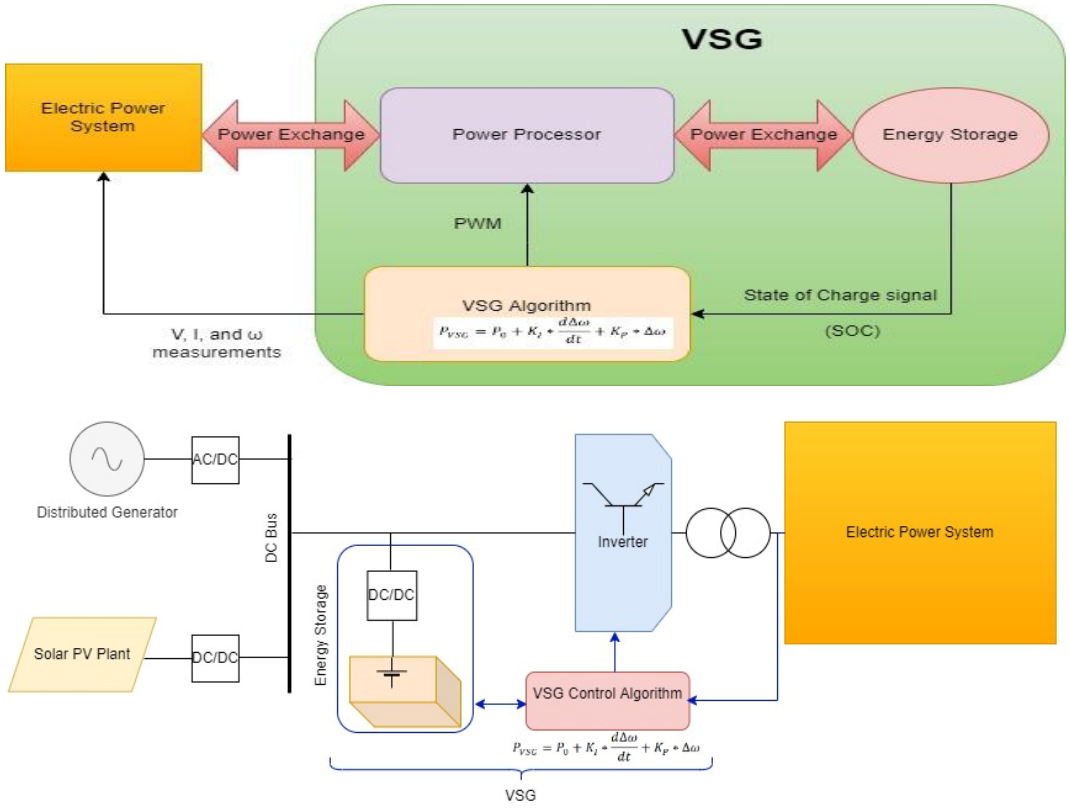

Figure 10. The VSG (a) concept and (b) general structure of VSG (reproduced from [23] and [22])

The early VSG concept was to reproduce the advantages offered by a SG in stability enhancement by imitating the dynamics properties of real SG. Single or multiple power electronics-based DG/ RES units can use the VSG principle in their connection with the grid. The VSG location is between DC bus/ source/ DG and the grid (seen in Figure 10 b). Active power through the inverter is controlled in inverse proportion of the rotor speed to emulate virtual inertia in the system. From the grid point of view, electromechanical SG and electrical VSG differ in electrical appearance only in terms of the higher frequency noise due to switching of inverter's power transistors. It is suggested that the VSG should also be able to absorb power, in addition to power injection. That would mean that in a stationary situation, the VSG's energy storage should operate at about 50% of its nominal capacity[8]. The used energy storage technology will determine the limits of the state of charge (eg. 20% and 80% of maximum charge). Outside these limits, the VSG will work in virtual load mode, between these limits, the VSG is in active operation mode. The output power of VSG is described as follows:

$$P_{VSG} = P_0 + K_I * \frac{d\Delta\omega}{dt} + K_P * \Delta\omega \quad (10)$$

Where,

- $\Delta\omega = \omega - \omega_0$, ω_0 is the nominal frequency of the grid
- P_0: primary power that should be transferred to the inverter
- K_I, K_P: emulate the inertia and damper windings effect, respectively, in a SG

For the maximum specified frequency deviation and RoCoF, the VSG should exchange its maximum active power. This is done by the suitable setting of the negative constant gains, K_I and K_P. It is easy to see from equation (10) that increasing K_I and K_P will increase the power injected or absorbed for the same amount of RoCoF and frequency deviation, respectively. The important parameters to select the VSG's storage technology[9] for grid application are: *maximum power of the loads; maximum total response time delay*[10]*; control delay; detection time; average SOC at normal operation; and the power of the controllable generation units*. VSG equivalent inertia increases with increasing K_I. However, the inverter capacity and PLL accuracy impose a limit on

[8] This will have implications on the sizing of the energy storage capacity.
[9] Some possible non-synchronous storage technologies for delivering virtual inertia are given in Figure 7.
[10] The response time delay of VI is a principal difference from instantaneous response of RI. The effect of this delay on the sizing of energy storage/ inverters is demonstrated and discussed in Section 4.2.

the amount of inertia. The overload capacity of a synchronous machine is not offered by the inverter[11]. Thus, bigger power overshoots during transients (frequency deviations) result from a high derivative term, and the overload must be sustained by the inverter. The used Phase Locked Loops (PLL) determine the accuracy of the measured frequency. Therefore, a tradeoff between the virtual inertia, the inverter overload capacity, and the PLL characteristics is needed to obtain the optimum value of derivative term in (10).

As Microgrids (MG) integrate larger numbers of DGs with low or no inertia, VSGs have a crucial role in MG stability. Though, there is as yet no established literature giving the relation between the required VSG power (from all installed VSGs) and MG rated power. It is suggested that since VSGs largely support as primary control response, 5% of MG rated power as the VSG power could be appropriate, considering that in a power grid the amount of reserve power for secondary control is about 10-15% of total available power. [22]

In literature, the VSG is described as the most popular VI control topology among the different VI control topologies studied by Tamrakar et al. ([24]). As learned from this work, the underlying concept is like that described in Figure 10 for the different VI concepts, but the VSG control algorithm shown in Figure 10 can have different implements that are guided by the desired level of model sophistication and application. Four main VI control topologies described by Tamrakar et al. ([24]) are mentioned below-

1) *Virtual Synchronous Generators: A Frequency-Power Response Based Topology*
- As previously described, VSG mimics only the SG's inertia response of release/ absorption of KE, in response to frequency changes.

2) *Synchroverters: A Synchronous Generator Model Based Topology*
- The exact dynamics of a SG are replicated in this topology.

3) *Ise Lab's Topology: A Swing Equation Based Topology*
- This topology is similar to the Synchroverters, except it doesn't use the complete model of the SG, instead solving just the power frequency swing equation.

4) *Droop-Based Approaches*

[11] This would also be an important consideration when thinking between VI and RI.

- Unlike the previous set of approaches, this approach does not attempt to emulate the SG behaviour. Instead, frequency droop-based controllers are implemented with the assumption that the grid impedance is inductive, and the aim to operate isolated microgrid systems autonomously.

The detailed description of these topologies is not undertaken here. The performance comparison of these different VI control topologies shows that with appropriate parameter selection, all the topologies can achieve inertia response, and topology selection may be done depending of desired level of SG dynamics replication and application. To operate isolated power systems autonomously, the Synchroverter and Ise Lab's topology can provide grid-forming support and may be more suitable. On the other hand, for interconnected power systems, VSG topology, with its grid-following behaviour, is more apt. These control techniques, thus have different features and weaknesses in their quest to emulate inertia response – these topologies are collectively termed as 'First Generation'. The 'Second Generation' of research and development is driven to optimise and improve the VI system dynamics and stability from the grid's point-of-view and also, to minimize energy storage requirements. [24]

Energy storage requirement is the topic of the next reviewed paper. Sizing of the ESS required for VI is important for planning and cost feasibility.

Bera et al. ([25]), in anticipation of the development of a market for synthetic inertia in the future, provide a technical approach to sizing ESS for synthetic inertia. Grid inertial response from energy storage systems (ESS) is in the form virtual inertia from virtual synchronous generator (VSG). The sizing of ESS is proposed with a new methodology that considers the decrease in system inertia due to both RES penetration and various transmission line contingencies including component failures. A modified version of the reduced Western System Coordinating Council (WSCC) 9-bus test system is used to test and validate the proposed method. The details of this test system are not presented here but the proposed method is described. The steps in the method are as follows-

i. First, time-domain simulation (TDS) for all contingencies at all points of time of the study period is used to determine the minimum inertia level for maintaining system stability. The critical clearing times (CCT) are also determined for the disturbances.
ii. Then, sequential Monte Carlo Simulation is performed to determine the expected inertia of the system considering component failures.

iii. Finally, the minimum required inertia and the system inertia are compared at any point of time to determine expected sizes of ESS.

Results show that large ESS are required for low critical clearing times and long clearing times.[25]

Studies in this review until now have largely been about the theoretical view and considerations. This theory should be juxtaposed in context of the Transmission System Operators (TSOs) perspective, noting their constraints and plans for the way ahead. In the overall the power system, the TSOs are the best positioned to observe as well as evaluate solutions to the low inertia phenomena. The December 2020 report titled 'Inertia and Rate of Change of Frequency', by the European Network of Transmission System Operators ([26]) delves into the practical limits for inertia and RoCoF. The issue needs to be addressed in different time frames, from real time operation to planning stages. One technology solution among the report's conclusions and recommendations is synchronous condensers coupled with flywheels – this is a solution that can be provided LAES. Further, it is noted that the VI based on inverter applications will probably contribute to inertia, however, it is still uncertain the extent to which these solutions can fill the gap for the gradual decrease in inertia. The model and simulations developed in the next chapter bridge this uncertainty by way of quantifying the limits on VI capacity to replace the diminishing inertia, and the relative value of solutions such as LAES in filling this gap.

4. SIMULATION SCHEME AND RESULTS

As described in Section 1.4 and visualized in the Figure 9, the objective is to evolve a quantitative estimate of the relative VI capacity (that is the fast ESS + inverter capacity) needed to replace the decline in RI. Simulations are now developed to implement the discussed approach.

4.1 Simulation model development and reference model

Figure 11 shows the three different activities or phases encountered in the modeling process, namely, Theory, Practice and Solving Research Question.

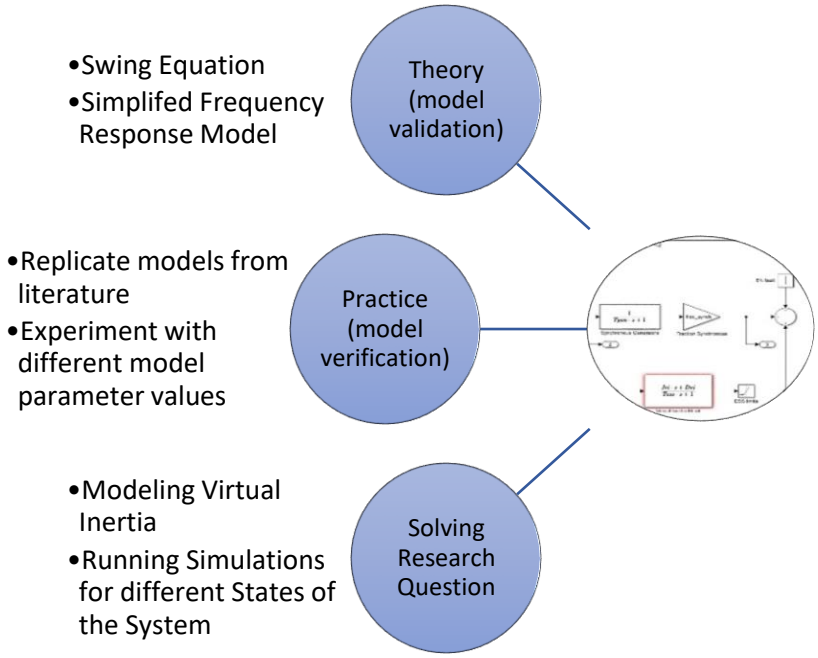

Figure 11. Phases of simulation model development

For simulation development, one approach is to replace the waning RI with the equivalent VI capacity size such that it results in a power system frequency response that is equivalent to the system with 100% synchronous generation (that is maximum possible RI). This implies, in case of a fault incidence, the RoCoF and / or frequency nadir in the system with a mix of VI and RI is equal or better than the system with 100% RI.

To develop this approach, first the frequency response of a 100% synchronous generation system, with nominal power system frequency of 50 Hz, is considered. This system is referred to as the reference power system and the corresponding frequency response as the reference frequency response. The reference frequency response is shown in Figure 12, for different sizes of faults in the power system.

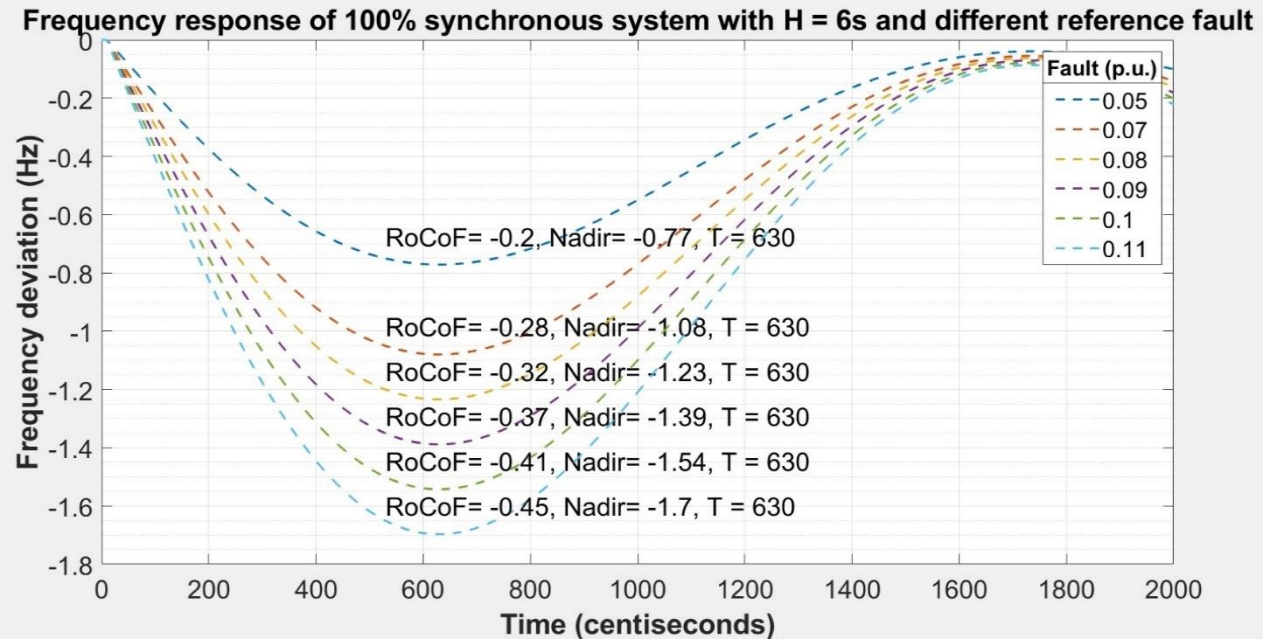

Figure 12. Frequency response of the 100% synchronous power system with inertia constant, H = 6s, for different sizes of the dimension fault. The frequency deviation is from the nominal power system frequency of 50 Hz.

This frequency response results from simulation of the power system frequency response model implemented in MATLAB/ Simulink (based on Figure 3.8 and Figure 6.9 in [27]) and shown in Figure 13. Studies show that the implemented system frequency response model, despite its simplicity, gives understanding of the way important system parameters affect the frequency response, particularly the RoCoF and frequency nadir after a major fault in the system. [28] , [29]. A comprehensive list of model components, their role in the model, the parameter value(s) and the reason behind the selected parameters is given in Table 9.

Some basics of the simulation runs are described next. At the start of the model, the power system is understood to have demand-supply balanced and there is no frequency deviation from the nominal value. At 0.1 seconds, a fault is introduced in the model, following which the frequency

deviation in the model is observed. The primary interest is in the frequency deviation in the initial seconds after a fault incidence, that is the RoCoF. In Figure 12, note that the duration of each run of the simulation is 20 seconds. The RoCoF, frequency nadir and the time of occurrence of the frequency nadir are shown in the figure, alongside the different frequency response curves, for different fault sizes. Interestingly, it is observed in the Figure 12 that the frequency nadir (maximum frequency deviation) occurs at T = 6.3 seconds (630 centi seconds) for all the different fault sizes. Indeed, the frequency response curves have identical movement along the time axis, albeit with different frequency deviations.

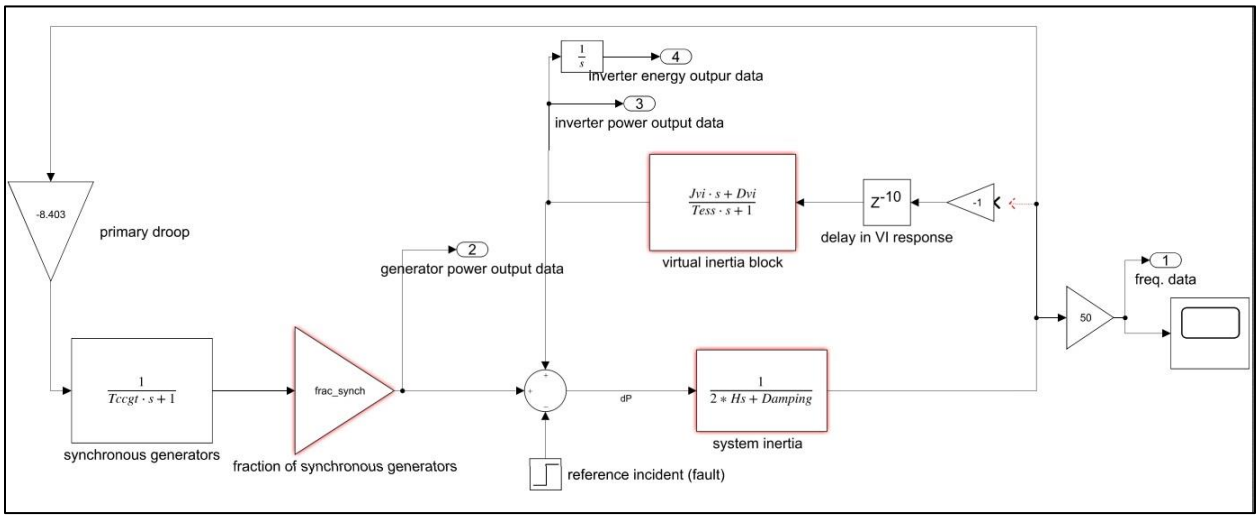

Figure 13. Simplified Power System Frequency Response Model, with virtual inertia block disconnected.

In the model shown in Figure 13, the virtual inertia block along with the preceding blocks (delay in VI response; -1 multiplier) is shown to be disconnected from the outer loop. This configuration is used to model the reference power system that has 100% synchronous generation. A simplistic assumption for the 100% synchronous generation system is that the equivalent generation is represented by combine-cycle gas turbine (CCGT) model. One reason for this assumption is that the common examples of low inertia power systems are the island power systems and an ever-increasing proportion of generating capacity on islands is understood to be comprised of CCGTs [30]. The equivalent inertia constant of this 100% synchronous generation system, $H = H_{max}$, is 6 s (the inertia constant of CCGTs is typically assumed to be 8 s which is a very high value among

synchronous generators), 6 s is considered to be a realistic and high inertia constant, sufficiently representative of 100% synchronous generation [31]. Frequency response shown in Figure 12 is for this reference system configuration.

The decline in system inertia is represented by the decline in the parameter value H from 100% synchronous generation value of 6 s to a steadily lower value from 5.5 s going down to 1.5 s. The parameter 'frac_synch', in the block 'fraction of synchronous generators' is defined to model the reduced primary frequency response available from the synchronous generators, as their fraction in the overall generation mix reduces[12]. It is defined as the ratio of the system inertia (H) to H_{max} (= 6 s), that is H / H_{max}. Thus, for the reference power system configuration this ratio is equal to 1.

Following are the steps in the modeling process flow-

1) First, the frequency response of the reference system is evaluated. Reference system has 100% synchronous generation with the system inertia constant of 6 s. The frequency response of this reference system is shown in Figure 12, for different sizes of the fault (0.05 p.u. to 0.11 p.u.). For example, in Figure 12, for a reference incident size of 0.05 p.u. (5% of base power system size), the RoCoF is -0.2 Hz/s, the frequency nadir is -0.77 Hz and the time of occurrence of the frequency nadir is 6.3 s.
2) Next, the declining RI trend and VI block are modeled. Decline in RI is caused by decline in the fraction of synchronous generation – this also leads to decline in the available primary frequency response from synchronous generation. To capture this the parameter 'frac_synch' has been defined. The 'frac_synch' parameter is defined as a ratio of system inertia constant and the inertia of 100% Synchronous system (6 s) i.e. frac_synch = H/H_{max} ('frac_synch' component is seen in the model in Figure 13).
3) Next, the VI block is added in the simplified frequency response model (based on equation 15 in [32], seen in the virtual inertia block in Figure 13).

$$\Delta P_{VI} = \frac{J_{VI}\, s + D_{VI}}{1 + sT_{ESS}} (\Delta f) \qquad (11)$$

[12] Whereas primary frequency response from synchronous generators is reduced, alternative sources of primary frequency responses may be procured by operators of a real grid. However, as mentioned in the earlier assumptions and limitations, this is not in the scope of the present study.

$where$

$\Delta P_{VI} = active\ power\ injection\ from\ the\ VI\ block$

$J_{VI} = virtual\ inertia\ constant$

$D_{VI} = virtual\ damping\ constant$

$T_{ESS} = time\ constant\ of\ the\ energy\ storage\ system$

$\Delta f = frequency\ deviation$

4) The RoCoF for different dimensioning faults in the reference system (Figure 12) are used as the benchmark for sizing the VI capacity under different simulations. For different lower (H) states, the VI constant, J_{VI} , is incremented step-wise in the simulation until the RoCoF for the resulting model is equal or greater than the reference system RoCoF.
5) Simulations are performed for variations in System Inertia, VI Delay and Dimensioning Fault. The scenarios are modeled for decreasing inertia in the range from 5.5 to 1.5, with steps of -0.5.

Table 9. Model components and parameter values

Sr. No.	Model Components	Component type and their role in the model	Component parameter(s) value	Reference/ reason for the chosen values
1.	'primary droop'	Gain function, it captures the change in power generation in case of demand-supply mismatch	-8.403	Approximate value chosen from suitable range
2.	'synchronous generators'	Transfer function; it is an aggregate of the response of different synchronous generators in the particular power grid	Tccgt = 8.68	Table 6.6 in [27]
3.	'frac_synch'	'Gain function'; it captures the trend of diminishing synchronous generation in the power grid	Different values iterated in the simulation, such that frac_synch = H(j)/Hmax H(j) is the selected inertia constant and Hmax is the maximum inertia constant. Hmax is set to 6s in the current study.	Captures diminishing inertia trend. The maximum system inertia constant, Hmax is set at 6 s.

4.	'reference incident'	'Step function'; it is maximum possible fault in the power grid.	Different values iterated depending upon the simulation, in the range of 5% to 11% (0.05 p.u. to 0.11 p.u.).	With more distributed generation, the 'reference incidents' are expected to be smaller than in the case of large scale 'centralised generation'
5.	'system inertia'	'Transfer function'; this block models the swing equation response of the power system	Different values iterated in the simulation for Inertia 'H'. The value for damping is set constant value of 0.1.	Damping constant, D [19]
6.	'delay in VI response'	'Delay block'; the different possible delays in the VI response are added to the model, before the 'Virtual Inertia block'	Different values iterated depending on the simulation, in the range of 0 ms to 210 ms.	[24], [22]
7.	'Virtual Inertia block'	'Transfer function'; the virtual inertia response is modeled here	The virtual damping constant is held constant at Dvi = 20; also Tess = 10. The VI constant, Jvi is the target variable. It values is incremented in the simulation until the frequency response (RoCoF) meets the reference system freq. response (RoCoF).	Adapted from Table 1 in [32]

This modeling process is summarized in Figure 14.

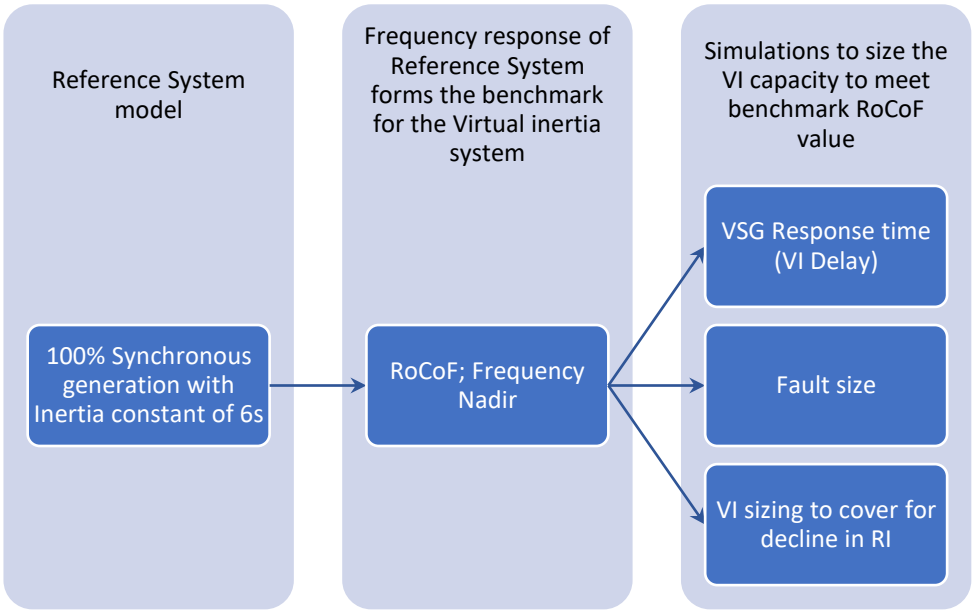

Figure 14. Modeling Process flow

Notes on model assumptions/ exceptions:

1) RoCoF Calculation

In the model, RoCoF is calculated[13] over a 500 ms time window which is a typical standard of RoCoF calculation in different grids. RoCoF calculation over different time windows (100 ms, 250 ms, 500 ms etc.) will result in different RoCoF values. Depending on the method of control of the VI unit, RoCoF could be an essential measurement. However, RoCoF as a control input is to be avoided because its measurement is challenging and highly susceptible to the power system disturbances. Appropriate standardization for RoCoF testing is still missing, despite the crucial nature of this parameter and multiple proposed measurement techniques. [33]

2) Very low frequency nadirs

The frequency responses in Figure 12 show very low frequency nadirs that would be considered impractical in real power systems. The RoCoF values are relatable (< 0.5 Hz/s), which is important for the inertial time scales focused in this study. The Operational Frequency Tolerance range in Table 2 may be consulted for reference frequency nadir values that can be tolerated in real power systems. The modeled system deviates from a typical power system model in that it does not have a secondary control loop and the primary droop control parameter values are within the range found in literature but not optimized for any scenario. The secondary control loop does not impact the frequency response in the initial seconds (RoCoF) after a major fault. This was further verified in trial model simulation runs with a secondary control loop.

3) Equivalent frequency response condition

The equivalent frequency response criteria, that is used to size VI that is needed to replace the diminished RI, is valid for the power systems where the system frequency is synchronously set by the rotational speed of synchronous generator rotors. If the percentage of synchronous generation in the system becomes so low that the frequency is no longer set by the synchronous generators

[13] Note that the RoCoF calculation is not required in the model of VI used (equation 11); it is only needed to compare the simulated frequency response with RoCoF calculated for the reference system frequency response.

but instead, is shaped by grid-forming inverters for example, then this assumption along with the role of inertia in the system will have to be reconsidered.

Also, initially both the RoCoF and Frequency Nadir criteria were set – in this case it was found that if the RoCoF criteria was achieved, the Nadir criteria was also achieved. Thereafter, only the RoCoF criteria was focused upon. Next, the different simulations and their results are discussed.

4.2 Simulation I: VSG response times (VI delay)

As noted in the literature review of [22], VSG's take a total maximum response time that includes time to detect frequency deviation, control delay and start time for power injection. Figure 15 shows the results for peak active-power needed from VSG to achieve the reference system RoCoF value (refer Figure 12) for different system inertia, as the VSG response times are varied. In this simulation, the reference fault-size is taken to be 0.07 p.u., the corresponding reference system RoCoF is -0.28 Hz/s. Note that this RoCoF criteria is the same for all the system inertia and response time values considered in this simulation. For declining system inertia values from 4.5 s to 2.5 s, the VI response time is varied from 0 ms to 120 ms in steps of 20 ms. As seen in the index in Figure 15, the different inertia states of the power system are shown by lines of different colours. Also, though the x-axis time scale is in centi seconds, in the text this time scale is referred in milli seconds (ms).

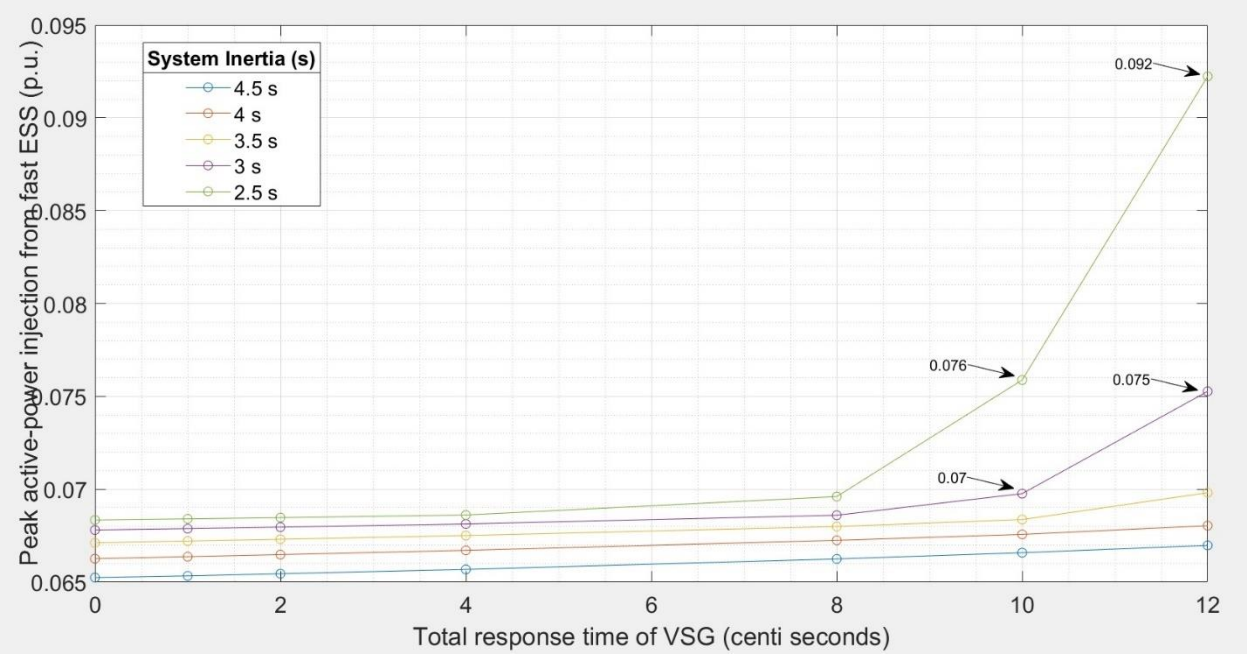

Figure 15. Peak active-power injection from fast ESS needed to match the reference power system RoCoF, for different states of system inertia, with variation in the total response times of VSG (Simulation I)

It is seen in Figure 15 that up to the system inertia of 4 s for all the response times and, till the VSG total response time of 80 ms for all the inertia states, the trend of increase in peak active-power injection is similar and relatively small. When this response time increases further to 100 ms and 120 ms, there is a sharp increase in the required peak power injection, particularly for the low inertia states of 2.5 s (green line) and 3 s (purple line). Thus, for a VSG delay of 120 ms and system inertia at 3 s, fast ESS with total peak power capacity of 0.075 p.u. is required to limit the RoCoF value to the reference system RoCoF value of -0.28 Hz/s. If the system inertia falls further to 2.5 s, the required fast ESS peak capacity value jumps to 0.092 p.u. Some points are marked in the Figure 15 that are equal or higher than the reference fault size of 0.07 p.u.

In the simulation results shown in Figure 16, a further lower system inertia of 2 s is also added in the simulation. As seen in the Figure 16, when the total response time of VSG increases from 100 ms to 120 ms, the graph for system inertia of 2 s makes a very large jump in value to the order of 10^4. In a real power system, either mitigation measures are expected to be in place that such a low inertia state does not arise in the power system, or the system would cascade to a blackout. The significant impact of 20 ms (100 ms to 120 ms) extra delay in VSG response and 0.5 s (2.5 s to 2 s) lower inertia on the power system is highlighted in this figure.

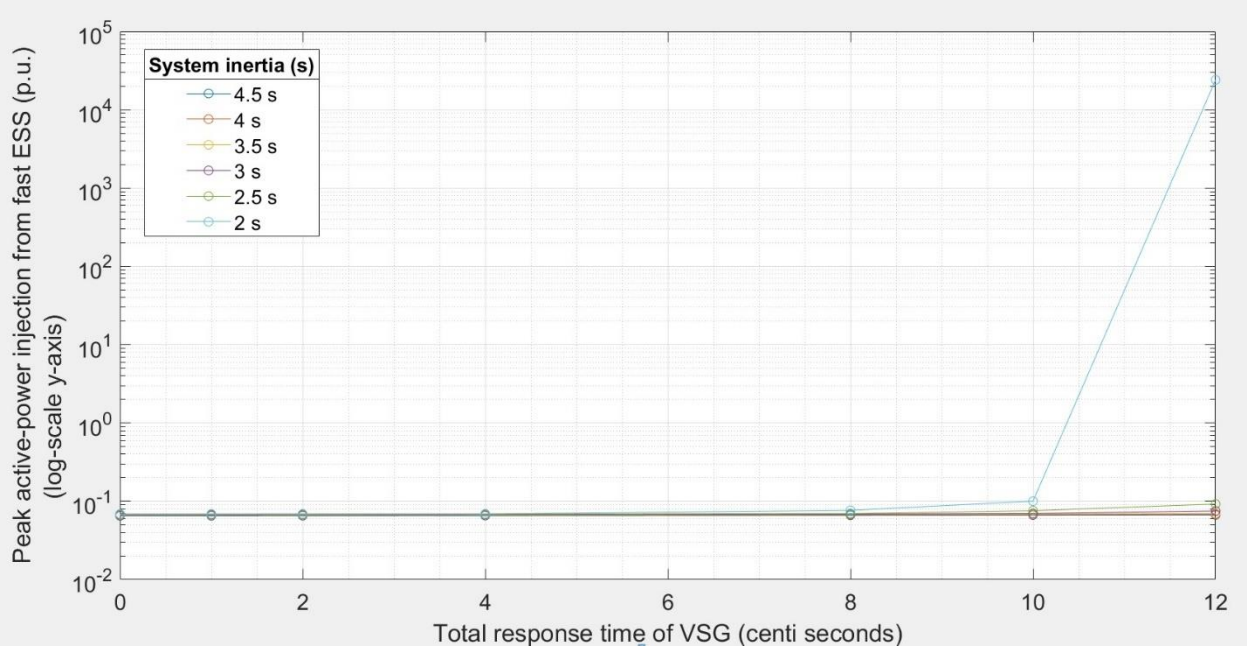

Figure 16. Peak power-injection from fast ESS jumps to a very high value when system inertia of 2 s is considered, and the VSG response time increases to 120 ms (Simulation I)

Figure 17 shows the final virtual inertia constant (J_{VI}) values at which the RoCoF criteria is satisfied and the simulation ends. The J_{VI} values increase as the total response time of VSG increases and the system inertia decreases.

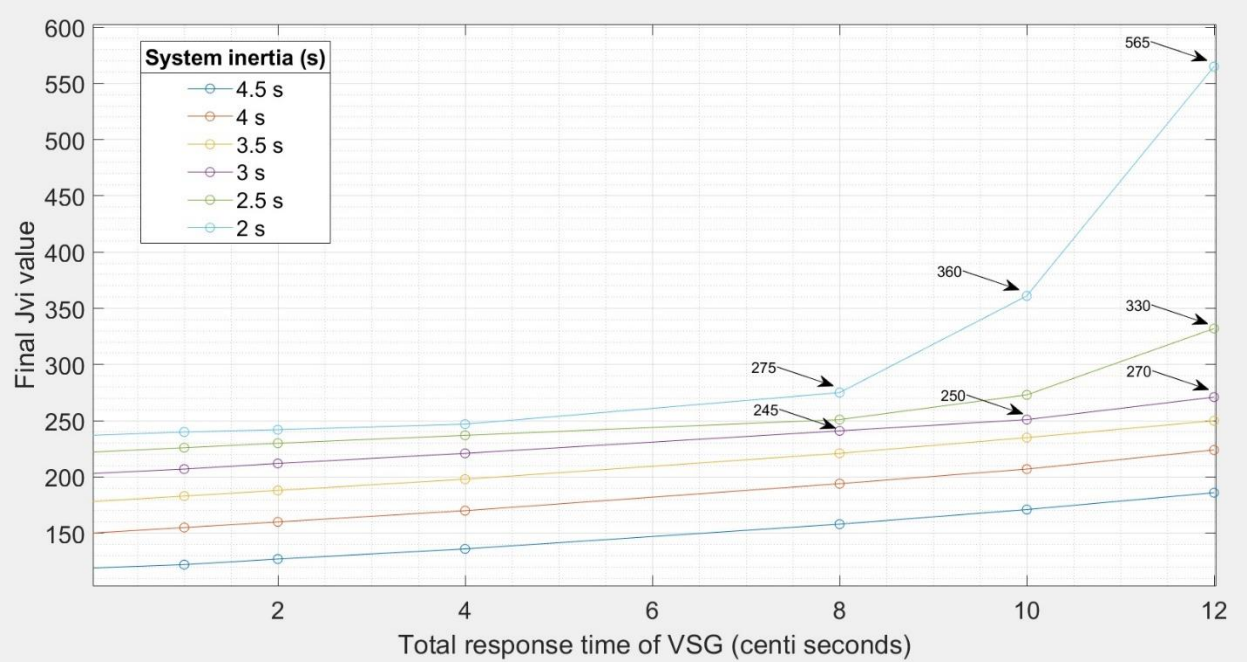

Figure 17. Final J_{VI} values needed to match the final reference power system RoCoF, for different total response times of VSG (Simulation I)

4.3 Simulation II: Fault sizes

Reference or dimension fault is the maximum possible fault-size in a power grid, for which the power grid is designed. Figure 18 shows the results for simulation of different reference fault sizes and system inertia. In this simulation, the VSG response time is taken to be 80 ms – this choice of response time is based on the results of the previous simulation (Figure 15), where it was noted that till the VSG total response time of 80 ms for all the inertia states, the trend of increase in peak active-power injection is similar and relatively small. Further, in the simulation of Figure 18, the reference fault size is varied from 0.05 p.u. to 0.11 p.u. and the system inertia value is varied from 5.5 s to 1.5 s. In departure from the previous Simulation I, where the RoCoF condition was the same throughout (- 0.28 Hz/s), in this Simulation II, the RoCoF condition is set separately for each reference fault size considered, as seen in Figure 12. This is because the as the reference fault size increases for the 100% synchronous reference power system, the RoCoF in the system will also increase. The reference fault sizes and the corresponding RoCoF's are noted in Table 10 below.

Table 10. Reference fault sizes and the corresponding RoCoF values in the 100% synchronous reference power system

Reference fault size (p.u.)	0.05	0.07	0.08	0.09	0.10	0.11
RoCoF (Hz/s)	-0.20	-0.28	-0.32	-0.37	-0.41	-0.45

Returning to the results seen in Figure 18, the trend for peak active-power injection jumps in value when the inertia drops to 2 s and has a much bigger jump when the inertia further drops to 1.5 s. For instance, for the reference fault of 0.09 p.u., as the system inertia declines from 2.5 s to 2 s to 1.5 s, the respective peak power injection jumps from 0.09 p.u. to 0.095 p.u. and finally to 0.145 p.u.

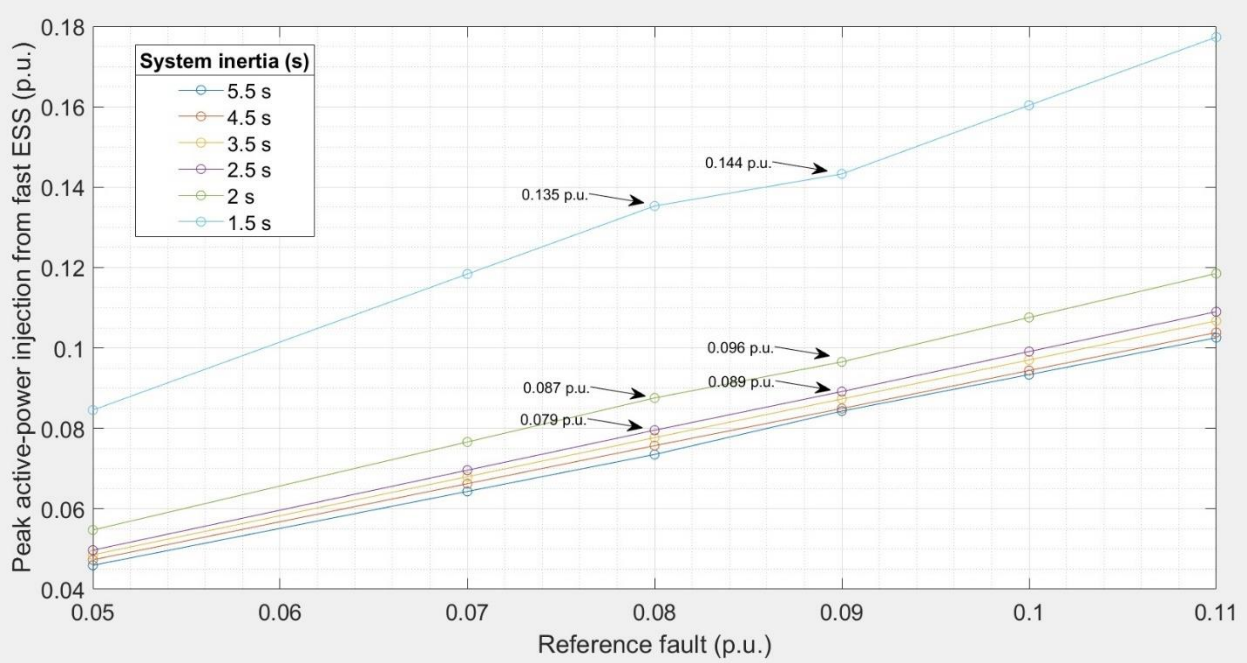

Figure 18. Peak active-power injection from fast ESS needed to match the reference power system RoCoF, for different reference fault sizes (Simulation II)

Corresponding to the simulation results in Figure 18, Figure 19 shows the final virtual inertia constant (J_{VI}) values at which the RoCoF condition is satisfied and the simulation ends.

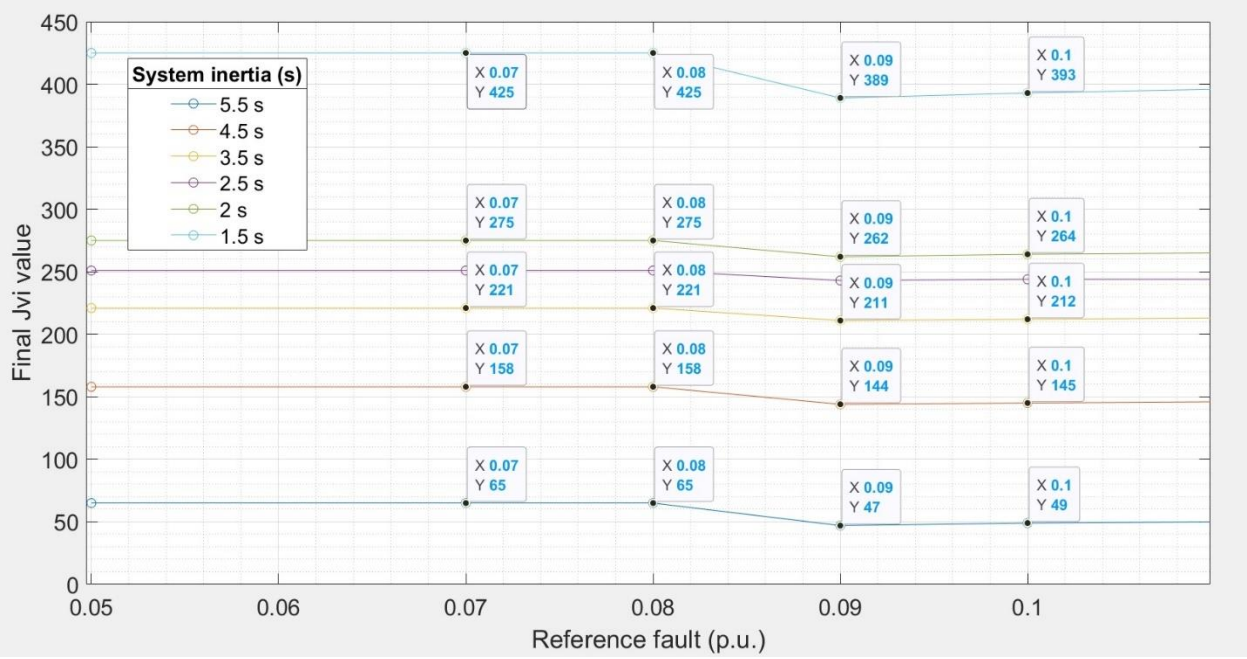

Figure 19. Final J_{VI} values needed to match the final reference power system RoCoF, for different reference faults (Simulation II)

In Figure 19, for each inertia state, the final J_{VI} value remains almost constant for the different reference faults. Interestingly, there is also a decrease in the J_{VI} value as the reference fault increases from 0.08 p.u., even though the peak active-power injection increases as seen in Figure 18. So, the decrease in J_{VI} means that the 's' term in Equation (10), representing the RoCoF, increases to a higher value such that the power output of VSG increases, even though the J_{VI} value decreases.

The RoCoF criteria is different for each reference fault size, and for a particular state of system inertia, it is noteworthy that J_{VI} values remain almost constant. This suggests that for a particular low inertia state, to be equivalent to 100% synchronous inertia system in terms of RoCoF response, the sizing of the VSG inverter, as it relates to the J_{VI} value, will be the same irrespective of the reference fault size. The required peak fast ESS capacity, however, will be higher as the reference fault size increases.

Note: Whereas the peak active-power injection indicates the required fast ESS capacity, the J_{VI} parameter is understood to be indicative of the required inverter capacity. The relation between J_{VI} parameter and inverter sizing needs further study and is not considered here.

4.4 Simulation III: Declining System Inertia and Required VI capacity, for different VSG response times

Simulation III looks at the relatively more percipient and instructive situation of declining system inertia, for different VSG response times. The reference fault-size, same as in the Simulation I, is taken to be 0.07 p.u. with the corresponding reference system RoCoF value -0.28 Hz/s. Figure 20, Figure 21 and Figure 22 show the results for different values of VSG response times and inertia.

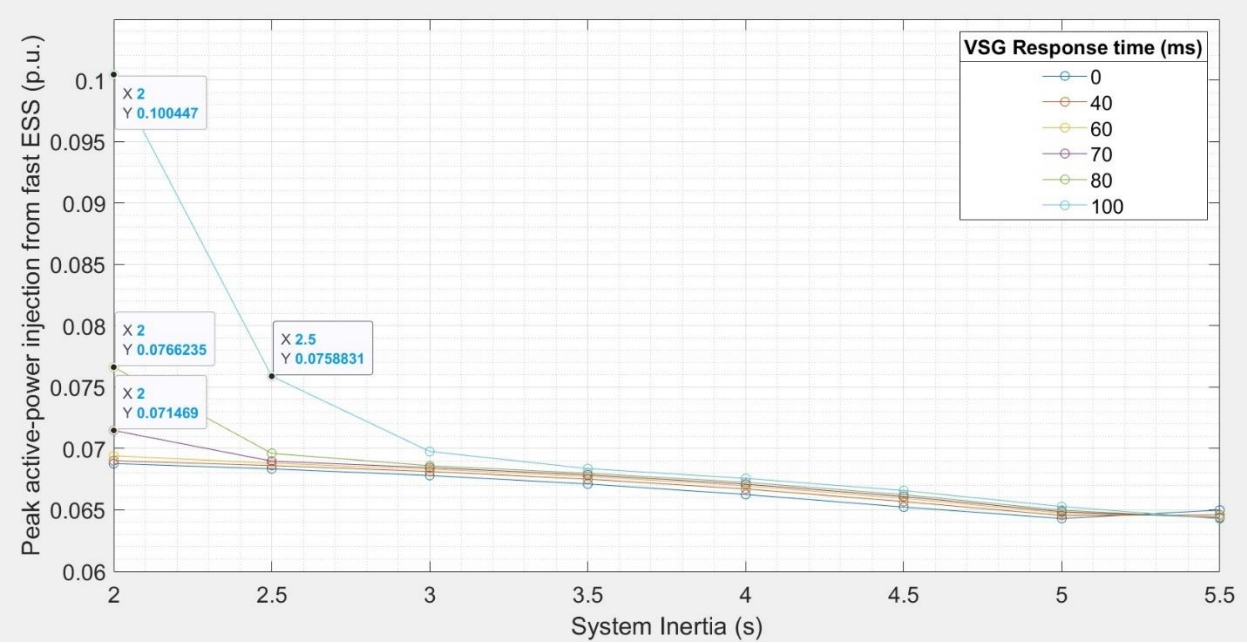

Figure 20. Simulation III results – from 0 ms up to 60 ms, the peak active-power is almost overlapping, from 70 ms the peak active-power starts to jump in value

Some observations from Figure 20, 21, 22 and 23 are-

1) Up to the VSG response time of 60 ms, there is no significant difference in the trend of peak active-power requirement from the high inertia of 5.5 s to rather low inertia of 2 s.
2) From Figure 20 and 21, it is seen that as the VSG response time increases, the rate of increase in the required peak active-power with declining inertia is faster.
3) From Figure 21 and 22, the steep rise in required peak power caused by additional 10 ms delay is highlighted as the inertia drops from 4 s to 3.5 s
4) Observe Figure 20 and Figure 23 - When the inertia is 5.5 s, the VSG with the lower response time has a slightly higher power output than the one with higher response times.

This power injection is not in line with observed trend for other values of inertia (this is seen a bit in Figure 20, but Figure 23 shows this more clearly). This is believed to be caused because 5.5 s is close to the reference system inertia of 6 s, the VSG providing earlier response may have greater opportunity to contribute. As more time passes (greater response time), a larger part of the required power may already be provided by the inertia response.

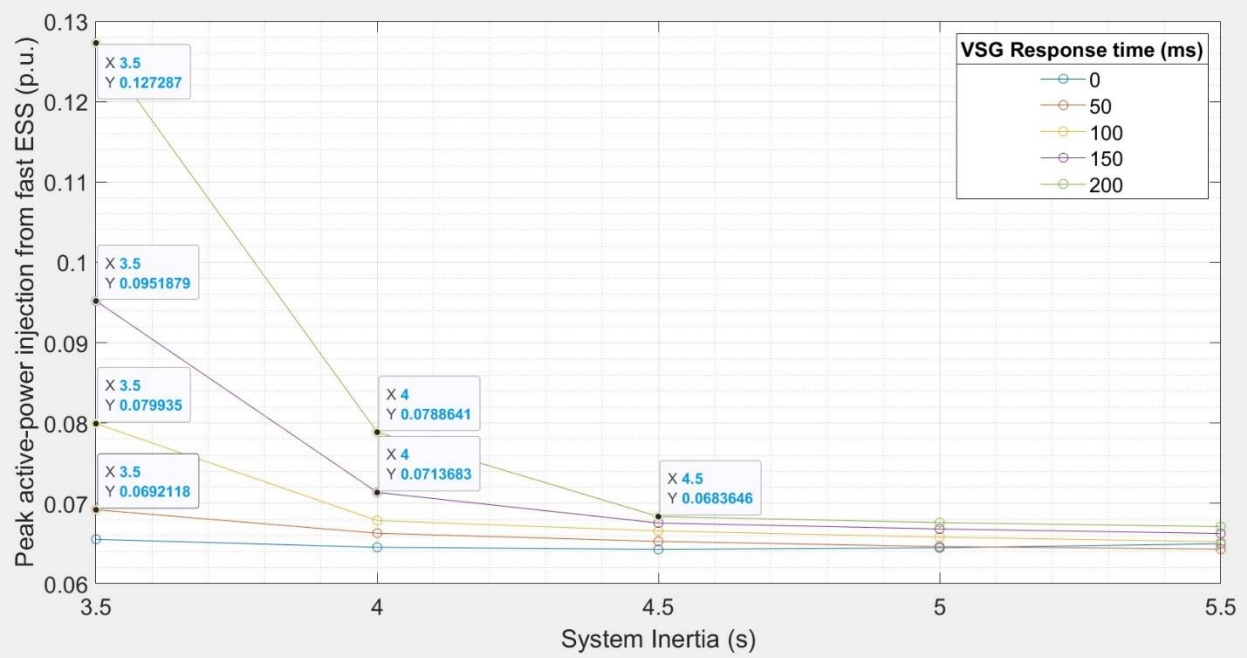

Figure 21. Simulation III results, with VSG response times increased up to 200 ms and system inertia limited to 3.5 s.

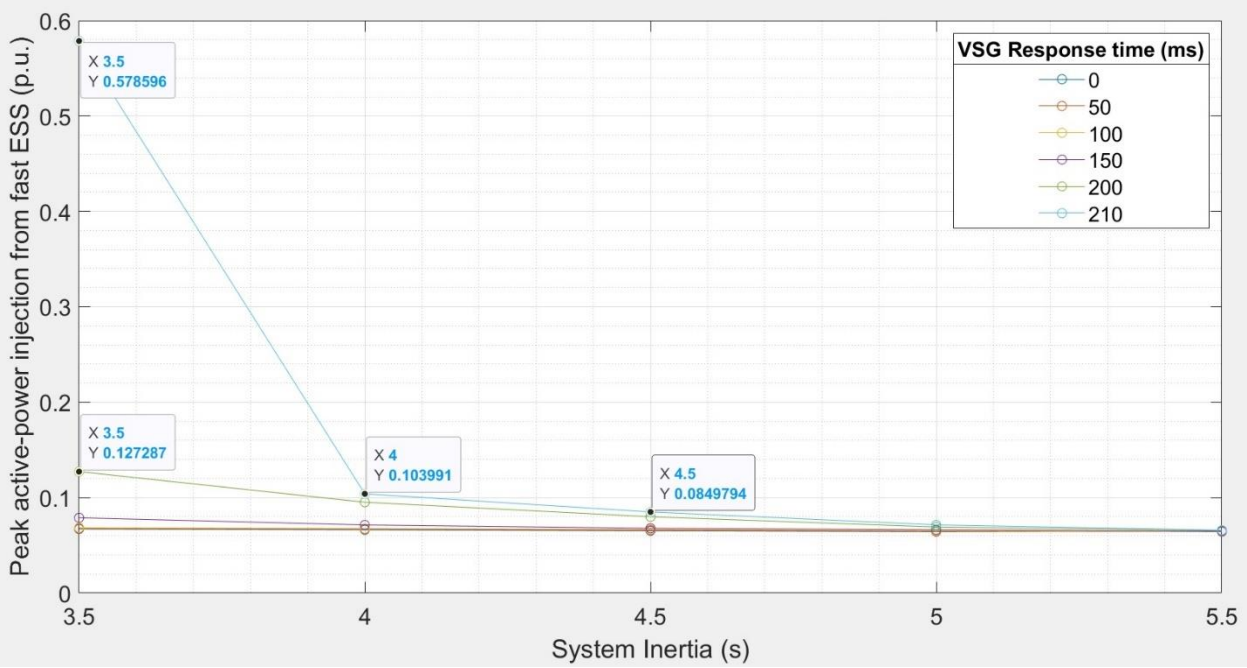

Figure 22. Simulation III results, with the maximum VSG response time increased by 10 ms, from 200 ms to 210 ms

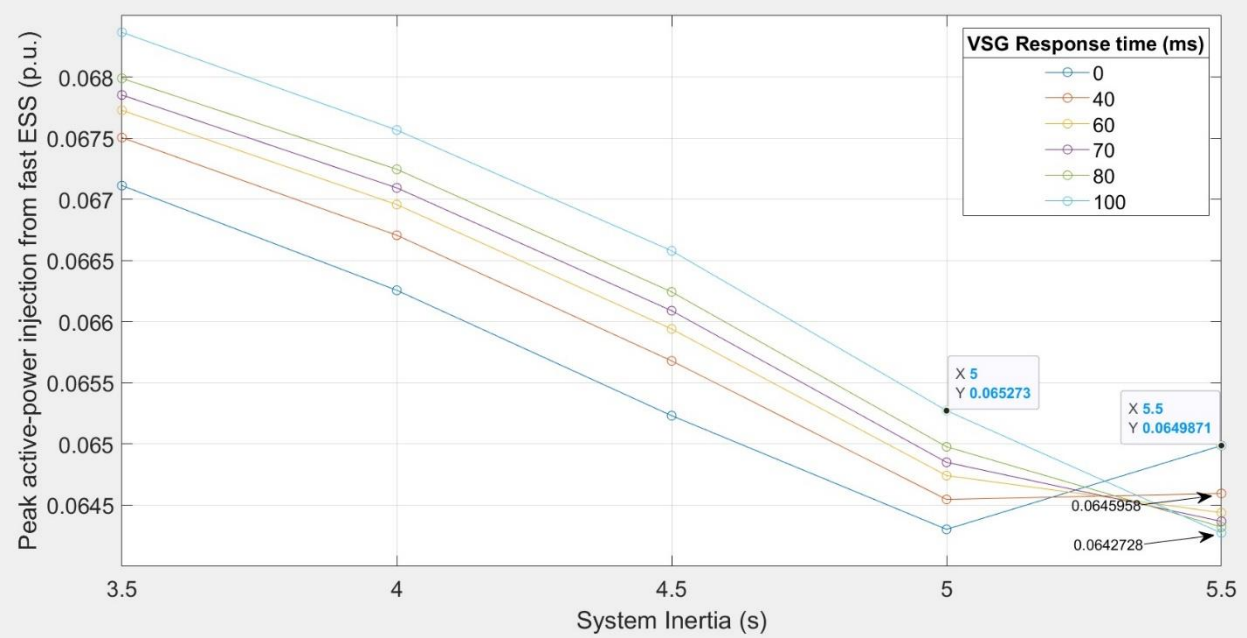

Figure 23. When system inertia is 5.5 s, the trend of peak active-power injection needed goes counter to the trend of the rest of the graph.

Figures 24 and 25 show the final J_{VI} corresponding to Figure 20 and 22 above, respectively. Simulation III. Consider Figure 22 and Figure 25 – even though peak active-power is much higher

for 210 ms than 200 ms at 3.5 s inertia, the J_{VI} values do not appear to be as widely separated. Whereas the peak active-power injection indicates the required fast ESS capacity, the J_{VI} parameter is understood to be indicative of the required inverter capacity. The relation between J_{VI} parameter and inverter sizing needs further study and is not considered here.

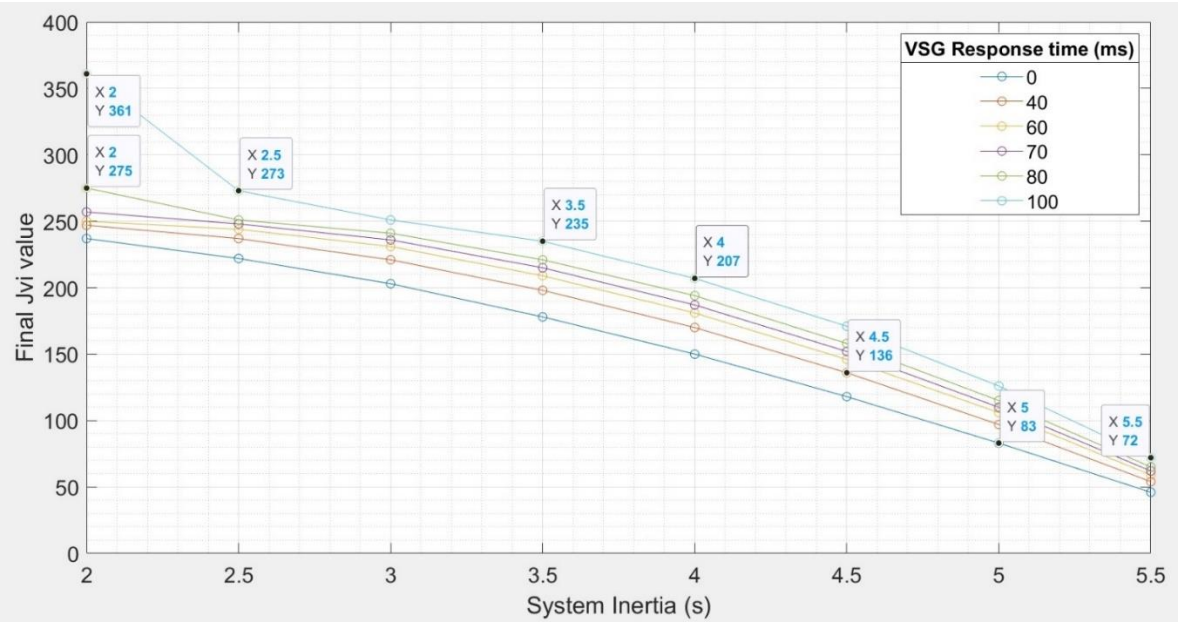

Figure 24. Simulation III, final J_{VI} values

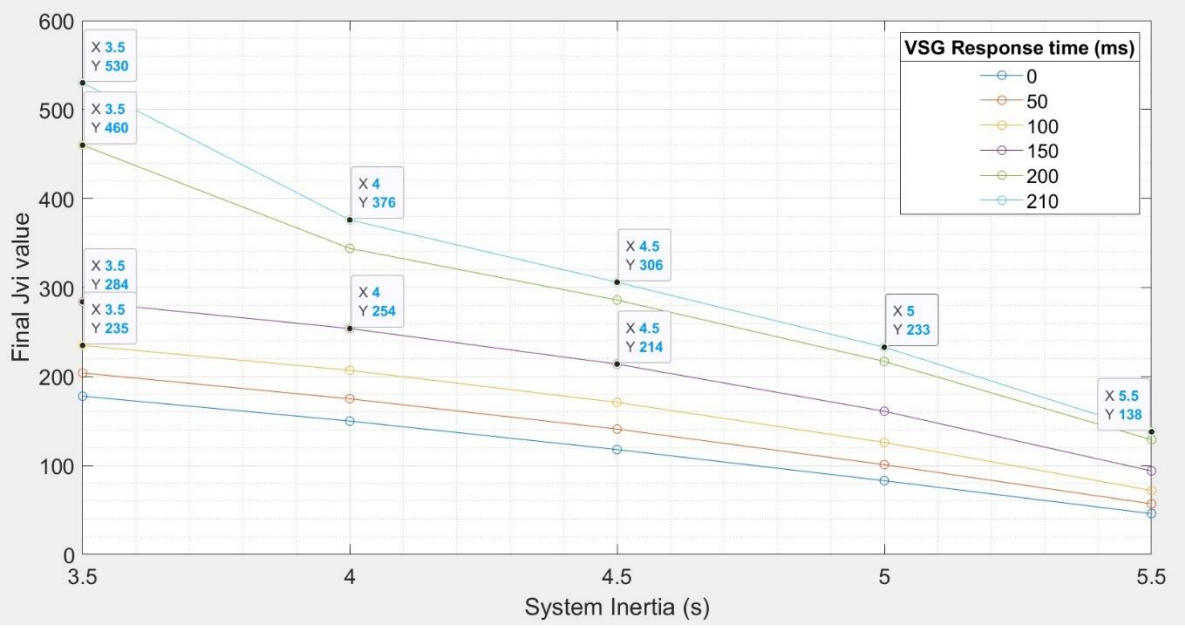

Figure 25. Simulation III, final J_{VI} values

4.5 Simulation IV: Declining System Inertia and Required VI capacity, for different fault sizes

Finally in this simulation, declining system inertia is considered, with different reference fault sizes. As noted in Simulation II (Table 10) the reference RoCoF is different for the different reference faults. The results for peak active-power injection are shown in Figure 26 and Figure 27 for two different VSG response times of 80 ms and 100 ms, with system inertia value being considered up to 1.5 s and 2 s, respectively.

Some observations from Figures 26 and 27 are-

1) The graph shape and trend are similar for all the different reference fault values.
2) The rate of increase in the required peak active-power injection increases, as the inertia declines.
3) As the VSG response time is increased from 80 ms to 100 ms, a similar graph pattern at an earlier system inertia value (2 s instead of 1.5 s).

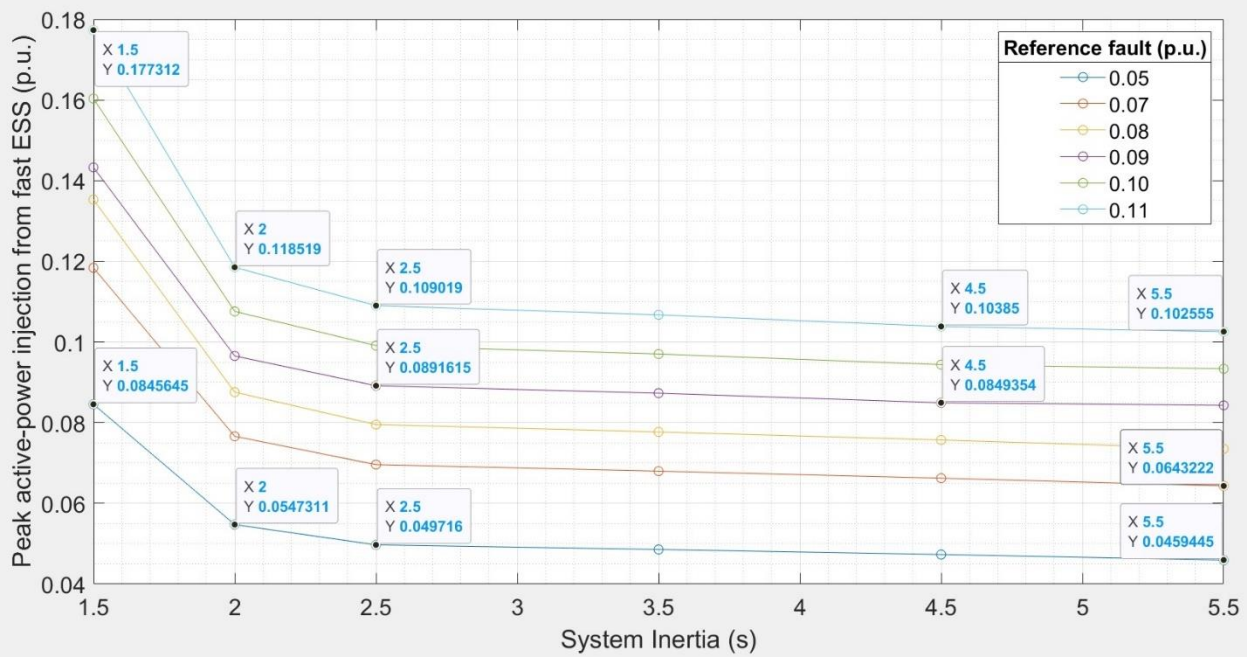

Figure 26. Simulation IV results, with VSG response time of 80 ms and system inertia going down to 1.5 s

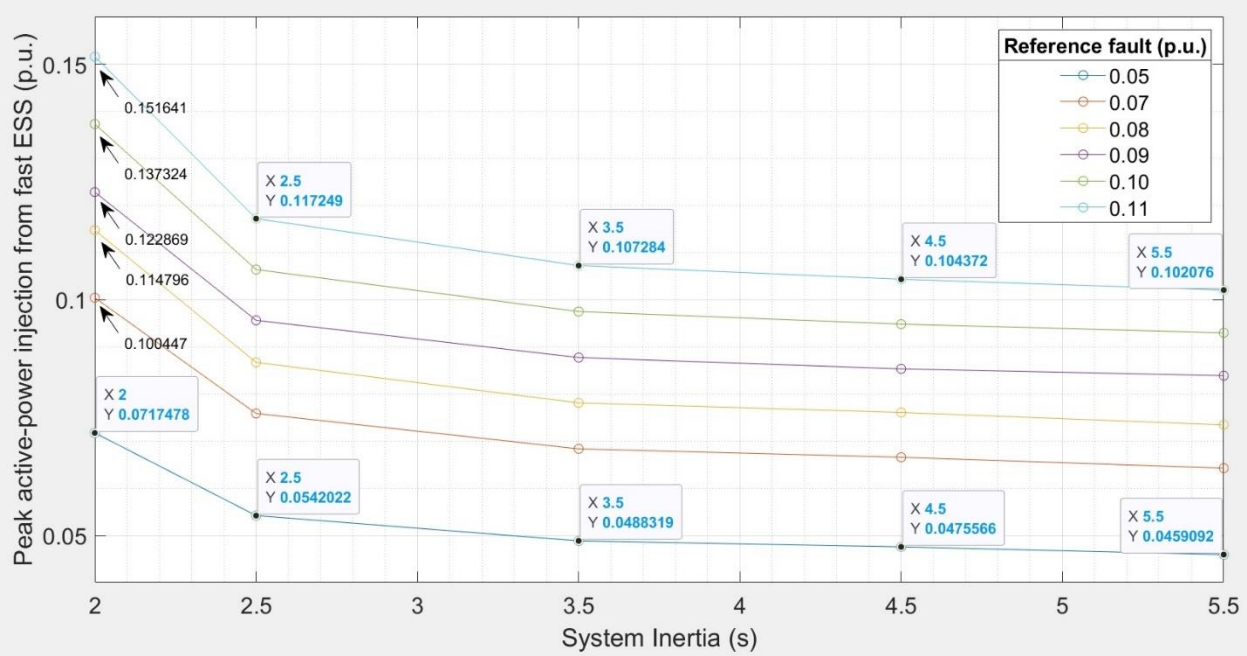

Figure 27. Simulation IV results, with VSG response time of 100 ms and system inertia going down to 2 s

The results for the final J_{VI} values corresponding to the figure 26 and 27, are shown in Figure 28 and 29, respectively. In both the graphs, the rate of increase in J_{VI} slows down upto some inertia (2 s, 2.5 s) and then shoots to a much higher value. Further, as noted in the results of Simulation II, the J_{VI} values remain almost constant for each inertia state, suggesting that to be equivalent to 100% synchronous system in terms of RoCoF response, the sizing of the VSG inverter, as it relates to the J_{VI} value, will be the same irrespective of the reference fault size. Also, in both figures 28 and 29, the graph for reference fault of 0.08 p.u. stands out from the other reference fault graphs which are all closely overlapping. This is unusual and not understood, it may result from some approximation or other inaccuracy.

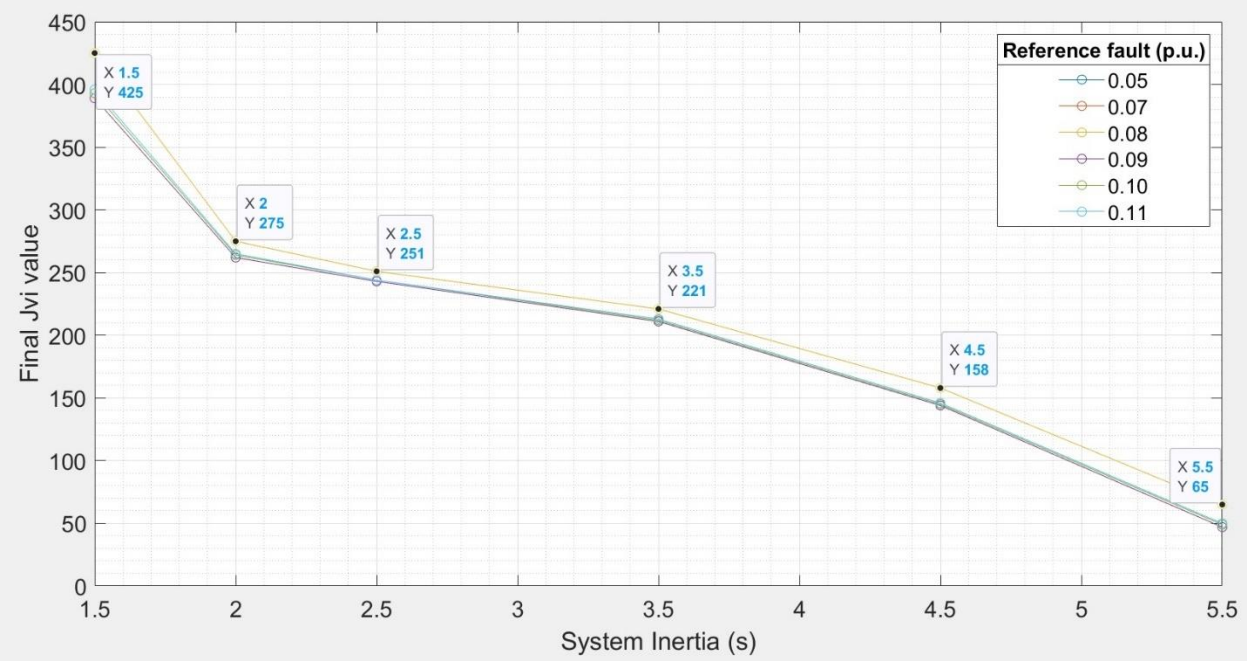

Figure 28. Simulation IV results, with VSG response time of 80 ms and system inertia going down to 1.5 s

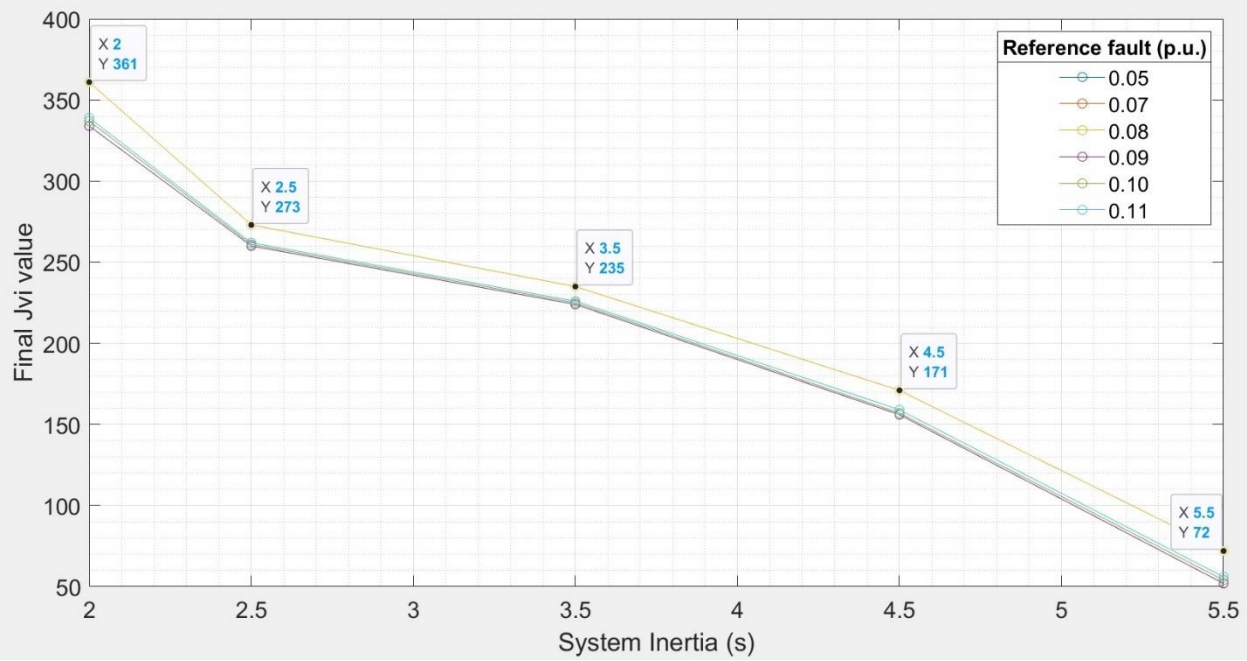

Figure 29. Simulation IV results, with VSG response time of 100 ms and system inertia going down to 2 s

5. REAL POWER SYSTEM CASE STUDIES

In this chapter, two real power grids are modelled, the Nordic grid and the Cyprus grid. The simulations in the previous chapter were conducted on a somewhat arbitrary power system model, as the focus was to examine VI capacity required at low inertia values; this exercise required running simulations until RoCoF conditions are met and it was computationally heavy. On the other hand, simulations of the real power systems were not as taxing computationally, but it required much more data and information to design the model for these real systems.

5.1 Nordic System

Nordic synchronous area comprises of TSO's from four countries- Finland, Sweden, Norway, and Denmark. In response to the trend of declining inertia, they have introduced a new fast reserve, Fast Frequency Reserve (FFR). FFR complements the existing primary reserve for disturbances (Frequency Containment Reserve, FCR-D) and takes over as the first mitigation measure at situations with low inertia and large reference incident. The FFR Market opened in May 2020. The different Nordic TSO's decided to start FFR procurement on their national markets, with the goal to later work towards a common Nordic FFR market. Based on the December 2019 report, Table 11 gives the market solution for FFR procurement in each of the national grids. [34]

Table 11 – Market solution for FFR Procurement for the four national grids in the Nordic Power system

National Grid	Market solution for FFR Procurement
Energinet (for DK2 only[14])	Proposed to be based on monthly capacity auctions until hourly procurement is possible
Fingrid	Hourly FFR market with daily procurement
Statnett	Seasonal market for FFR, providers can make offers for entire season or just for parts of the season
Svenska kraftnät	Seasonal procurement for 2020; Day-ahead procurement 2021 onwards

The national grids procure their contribution to FFR from their respective national markets and the total FFR procured (like other Frequency services such FCR-N/D) is pooled together with contributions from the four national grids. During the year 2020, the obligation of the respective national grids in the overall FFR procurement is given in Table 12. [34]

[14] Denmark's national grid is divided in two synchronous areas – only one of these areas, DK2, is synchronized with the Nordic power system.

Table 12 – Division of Nordic FFR procurement obligations to the different TSO (reproduced from Table 3 in [34])

FFR sharing key	Energinet	Fingrid	Statnett	Svenska karftnat
Obligation [%]	14	20	42	24

In response to frequency deviation, FFR has three alternatives for full activation time for active power support – these times are 0.7 s, 1 s and 1.3 s. These activation times correspond to different frequency activation levels – Table 13 shows the three alternative combinations of these two values. Also, the short support duration and long support duration are respectively, 5.0 s and 30 s. [34]

Table 13: Three alternatives for the combination of frequency activation level and full activation time for FFR (reproduced from Table 1 in [34])

Alternative	Activation level (Hz)	Maximum full activation time (s)
A	49.7	1.30
B	49.6	1.00
C	49.5	0.70

Like the previous simulations, the modeling objective here is understanding the relative competitiveness of direct inertia (synchronous rotational inertia) procurement to other solutions for inertia compensation. In the previous simulations, the general VI concept and VSG were considered, FFR will be considered in the present case. Initially only the model representation of the Finnish electrical grid was planned, and not the entire Nordic synchronous area. However, after modeling with parameters restricted to Fingrid and reflecting on the model and the results, it became evident that it is not justifiable to consider frequency response and inertia in isolation only for the Finnish grid. Inertia is a common property of the Nordic power system, spreading beyond the market boundaries of the individual national grids. So, modeling the frequency response of Finnish electrical grid in isolation from rest of the synchronously connected Nordic power system is not meaningful.

At the same time, for the present analysis only the FFR procured in Fingrid is considered in the model. This is for reasons of simplicity and also because the relative competitiveness of alternative FFR solutions vis-à-vis direct inertia procurement is expected to differ among markets, given the

differences in FFR procurement volume, market structures as well as prevailing considerations of the national grids. As shown in Table 11, Fingrid has an hourly FFR market with daily procurement. In those time intervals, data is available for the FFR procured, the system kinetic energy, the production, consumption, and transmission data. Table 14 shows an indicative sample of the datasets available from the Fingrid open data portal (data.fingrid.fi/en/).

Table 14: Sample of the datasets available on the Fingrid open data portal (data.fingrid.fi/en/)

No.	Dataset	Unit	Data period	Data Description
1.	Kinetic energy of the Nordic electricity system – real-time data	1 GWs	1 min	Real-time estimate of the kinetic energy of the Nordic power system calculated by the Nordic transmission system operators.
2.	Fast Frequency reserve FFR, procurement forecast	MW	1 h	The procurement prognosis for Fast Frequency Reserve (FFR) (MW). Fingrid procures FFR based on the procurement prognosis. The prognosis is updated once a day, typically at 11:00 (EET).
3.	Fast Frequency reserve FFR, procured volume	1 MW	1 h	The volume of procured Fast Frequency Reserve (FFR). The procured volume will be published 22:00 (EET) on previous evening.
4.	Fast Frequency reserve FFR, price	€/MW	1 h	The price of procured Fast Frequency Reserve (FFR) (€/MW). The price will be published 22:00 (EET) on previous evening. The price is determined by the price of the most expensive procured bid (marginal pricing).

The summer months of July and August are seen to have among the lowest kinetic energy (inertia) in the year. Maximum FFR would be procured when the system is expecting to have the least kinetic energy reserve. For the month of August 2021, the maximum FFR procured was 62.4 MW and it was from 4 AM to 6 AM on the morning of 22nd August 2021. This period of maximum FFR procurement was chosen to simulate the low inertia state for the Nordic power system, particularly the instant of 05:01:00 AM. The available real-time parameter values at the instance of the simulation are tabulated in Table 15 and values for other Nordic grids that could not be found and were approximately calculated are shown in Table 16.

Two different models of the Nordic Power system frequency response are implemented and simulated. First model, shown in Figure 30, follows the similar approach as in the previous model simulated in Chapter 4 but with separate steam turbines and hydro turbines, representing Fingrid and the other Nordic grids. The second model, shown in Figure 33, is adapted from the paper [35]

– this model is tuned based on real events in the Nordic power system for real-time estimation of frequency stability. Result of both these models are discussed next.

Table 15. Power system data for Fingrid and Nordic grids on 22nd August, 2021 at 05:01:00 hours

	Parameter	**Value (MW)**	**Comment**
	Total Nordic Grid Electricity consumption	31476	
	Frequency	49.924	Unit is Hz
	Real time Kinetic energy estimate of the FinGrid Power System	138	Unit is GWs
Data for Fingrid			
	Electricity consumption	7267	
	Electricity production	5896.8	
	Wind power production	943.95	
	Industrial cogeneration	1312	
	Cogeneration of district heating	286	
	Nuclear power production	2685.2	
	Electricity production, reserve power plants and small-scale production	45	
	Peak load power	0	
	Hydro power production	627.67	
	Transmission between Finland and Norway	-39.425	
	Transmission between Finland and Estonia	1029.1	
	Transmission between Finland and Russia	-1402.7	Reference incident
	Transmission between Sweden and Åland	-16.2	
	Transmission between Finland and Central Sweden	-400.2	
	Transmission between Finland and Northern Sweden	-579.33	
	FFR Reserve Acquistion Volume	62.4	
	Real time Kinetic energy estimate of the FinGrid Power System	30.09	Unit is GWs
	FCR-D Procured Volume in hourly market	66.6	
	FCR-D reserve plans in the yearly market	312.7	
	Total FCR-D	379.3	
	FCR-N, hourly market volumes	20	
	FCR-N, yearly market plans	68	
	FCR-N, Foreign trade	35	
	Total FCR-N	123	

Table 16. Approximate data for other Nordic grids, based on available data (in MW)

	Total	Wind	Total - Wind	Approx. proportion		Approx. Hydro	Approx. Steam
				Hydro	Steam		
Sweden	12469	2536	9933	0.59	0.41	5860.47	4072.53
Norway	11049	0	11049	0.934	0.066	10319.8	729.23
DK2	193	80	113	0	1	0	113

5.1.1 Nordic Power System – Model 1

Figure 30 shows the Nordic Power system model-1 implementation. Figures 31 and 32 show the results of this model. The reference fault incident in the simulation is taken to be the power transmission between Finland and Russia. Its value at the instant of the simulation, as seen in Table 15, is 1402.7 MW with the power being exported by Russia and imported into Finland. This is the maximum possible contingency event in Fingrid. With the total Nordic electricity consumption base of 31476 MW (Table 14), the p.u. size of this reference incident = $\frac{1402.7}{31476}$ = 0.045 p.u. The frequency response observed in Figures 31 and 32 are for this reference fault size.

Also, the existing kinetic energy reserve of 138 GWs of the Nordic Power system (Table 15) results in a system inertia value of $\frac{138*1000}{31476} = 4.38\ s$.

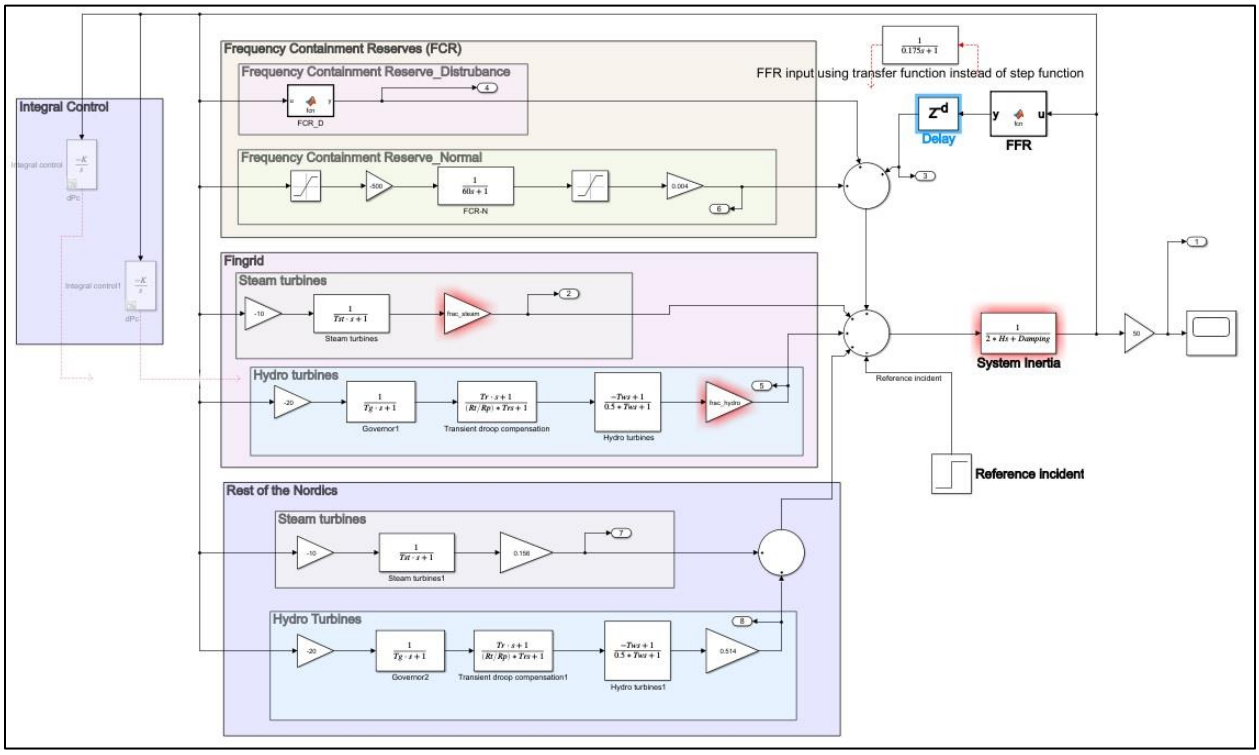

Figure 30. Nordic Power system – model 1

The inertia value of 4.38 s is incremented up to 4.68 s, in steps of 0.05, as seen in the index of Figure 31 and the RoCoF and Nadir are documented for each inertia value. As shown in the Figure 31, as the system inertia increases from 4.38 s to 4.68 s, the absolute RoCoF value decreases from 0.26 Hz/s to 0.24 Hz/s and the absolute Nadir value decreases from 0.68 Hz to 0.66 Hz. In kinetic energy terms, a 0.1 increase in system inertia from 4.38 s to 4.48 s would require raising the kinetic energy reserve by $\frac{0.1*31476}{1000} = 3.1476\ GWs$, for the system base of 31476 MW (in the model, the system base is taken to be the total Nordic electricity consumption at the time of simulation, Table 15). This is roughly equal to 10% of the existing KE reserve for Finland which is 30.09 GWs (Table 15).

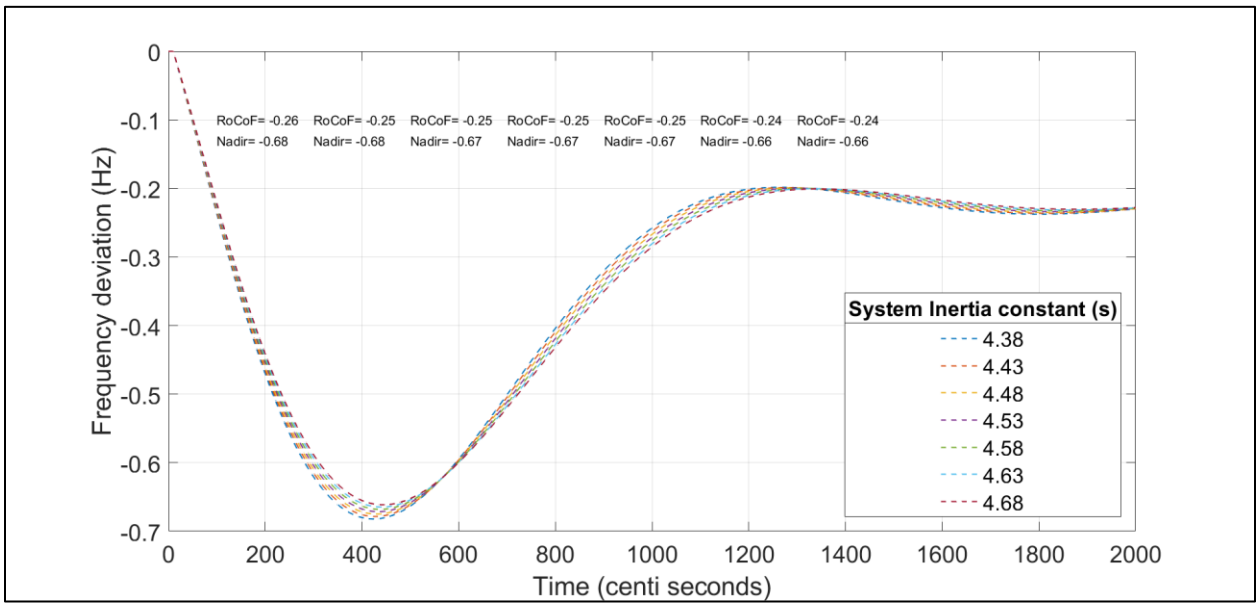

Figure 31. RoCoF and Nadir values after reference incident in the Nordic power system (Model 1) for constant increments in the system inertia values from 4.38 s to 4.68 s.

Next, Figure 32 shows the simulation results for the activation of 62.4 MW of FFR, with the inertia set at its actual value of 4.38 s. The simulation is performed for the three different FFR alternatives as per Table 13. As seen in the Figure 32, the RoCoF value for all the three FFR alternatives

remains at -0.26 Hz/s. The alternative with maximum activation time of 1.3 s results in a frequency Nadir of -0.66 Hz, whereas for the other two alternatives, the frequency Nadir is -0.67 Hz.

Some observations from comparing the results in Figure 31 and 32:

1. The FFR of 62.4 MW achieves a frequency deviation that requires increment in system inertia of 0.1 for -0.67 Hz, and 0.25 for -0.6 Hz. As mentioned earlier, 0.1 increment in system inertia implies increasing KE reserve by 3.1476 GWs.
2. The increment in system inertia diminishes the RoCoF values, but the FFR does not affect the RoCoF values.

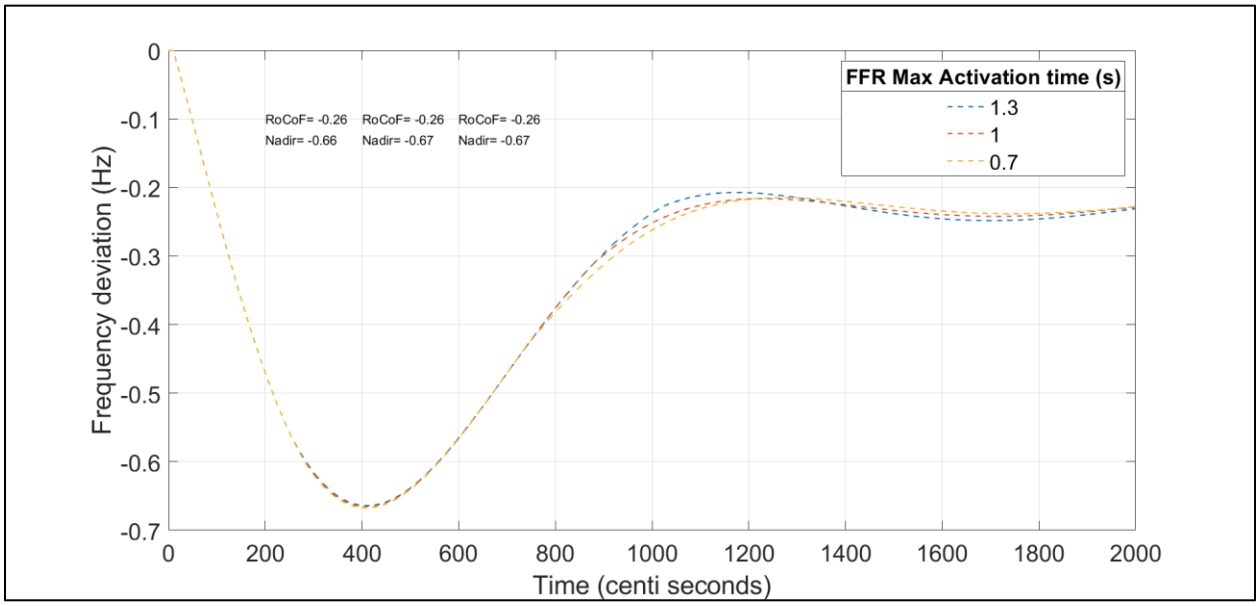

Figure 32. RoCoF and Nadir values after reference incident in the Nordic power system (Model 1) for three different alternative FFR options, and with system inertia at its actual value of 4.38 s.

5.1.2 Nordic Power System Tuned Model-2

Figure 33 shows the implementation of the Nordic Power System Model-2, taken from the reference [35]. This model also uses the value from the same time instant as in the previous model.

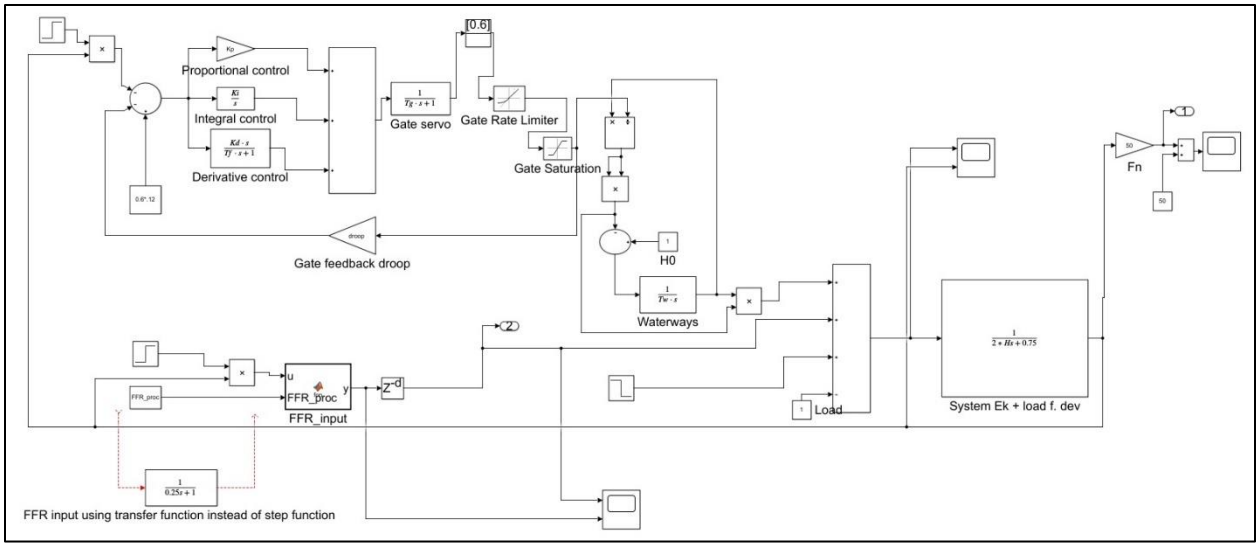

Figure 33. Nordic Power system tuned model 2 [35]

Though the results for this simulation, shown in Figure 34, are somewhat different from results in Figure 31 and 32. The results of this simulation are expected to be more accurate representation of the actual Nordic system, as this model is especially tuned taken real events in the Nordic system into account.

As seen from the results in Figure 34, in this simulation the inertia is incremented directly as KE reserve instead of inertia values. Further, in addition to the actual FFR procured of 62.4 MW, FFR values that are twice (124.8 MW) and five-times (312 MW) are also simulated. The FFR modeled in this result is the Alternative C in Table 13.

Some observations from the Figure 34 are:

1. Note the time of occurrence of frequency nadir, T, in the figure. As system KE is increased, the occurrence of frequency nadir gets delayed. On the other hand, as FFR is increased, the frequency nadir occurs earlier.
2. Increments in KE improve RoCoF value, but even with five times the actual FFR value (312 MW), there is no change in the RoCoF value.
3. 62.4 MW of FFR results in the same frequency nadir as 30% increment in KE reserve from system base (= 0.3 x 31476 = 9442.8 MW s = 9.44 GWs).

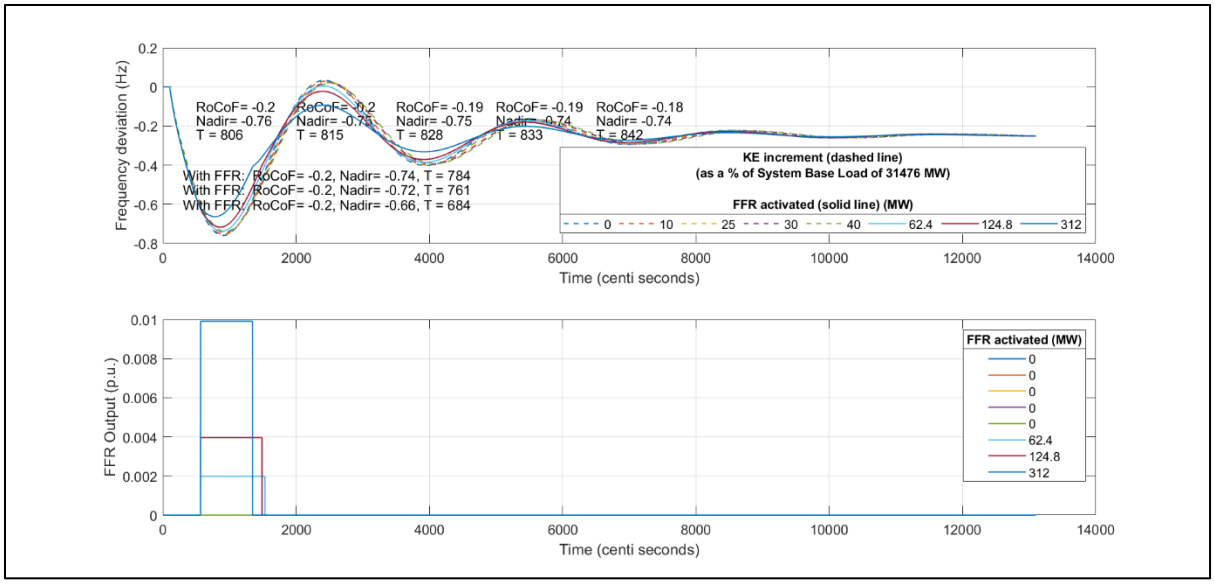

Figure 34. RoCoF and Nadir values after reference incident in the Nordic power system (Model 2). Here, simulation of KE increment is followed by simulation of FFR activation. In the top figure, the dashed line shows the different KE increments, and the solid line shows the different FFR activation. The bottom figure visualizes the different FFR power activation – the initial '0' values in the index are when the KE increment is simulated with the FFR activation set to 0.

5.2 Exploratory modeling of LAES operation in Cyprus Power Grid

Exploratory modeling and analysis are performed for the context of the Cyprus power grid. The Table 17 lists the different power stations comprising the Cyprus Power Grid and Table 18 shows the steady rise in the proportion of renewable energy sources in Cyprus electricity generation.

Table 17: Power Generation capacity from Conventional Fuels comprising the Cyprus Power Grid ([36])

Power Station	Fuel	Maximum Capacity
Vasilikos Power Station		**868 MW**
3 x 130 MW Steam Units	Heavy Fuel Oil	390 MW
1 x 38 MW Open Cycle Gas Turbine	Gas Oil	38 MW
2 x 220 MW Combined Cycle Gas Turbine Units	Gas Oil	440 MW
Dhekelia Power Station[15]		**460 MW**
6 x 60 MW Steam Units	Heavy Fuel Oil	360 MW
2 x 50 MW Internal Combustion Units	Light Fuel Oil	100 MW
Moni Power Station		**150 MW**
4 x 37.5 MW Open Cycle Gas Turbines	Gas Oil	150 MW
Mari Power Station[16]		**260 MW**
260 MW Combined Cycle Gas Turbine	Liquified Natural Gas	260 MW

Unlike the Nordic System, Cyprus is an island with very limited assets in the grid and a competitive market model such as the Nordic FFR market will not work for Cyprus. It is therefore required that the future infrastructure needs of the overall Cyprus grid are considered in the planning stages. For this reason, we build a scenario for a fully renewable future Cyprus grid and envision Liquid Air Energy Storage (LAES) systems supporting this grid by provisioning energy storage capacity and rotational inertia to the grid. The idea is to investigate the scope and size of LAES in supporting the frequency stability of this grid in future generation scenarios.

[15] Dhekelia Power station is to be decommissioned in 2024 [36]
[16] Mari power station is anticipated to be in full operation in 2023 [36]

Table 18: Year wise percentage of electricity generation from renewable energy sources ([37])

Year	RES total	Distribution system connected			Transmission system connected	Conventional Fuels
		Solar PV	Biomass	Wind	Wind	
2011	3.31	0.2	0.8	0	2.3	
2012	5.24	0.4	0.8	0.04	3.9	
2013	7.5	1.1	0.8	0.1	5.5	
2014	7.0	1.9	0.9	0.1	4.2	
2015	8.5	2.8	0.8	0.1	4.8	91.6
2016	8.4	3.0	0.8	0.1	4.6	91.7
2017	8.4	3.4	0.7	0.04	4.2	91.6
2018	9.0	3.9	0.7	0.04	4.3	91.2
2019	9.7	4.2	0.8	0.04	4.6	90.5
2020	11.7	5.8	0.9	0.04	5	88.1

Figure 35 shows the basic representative model of the Cyprus system, with the LAES model also added in the system. Attempt was made to find / calculate the suitable 'Time Constant' value for LAES system. LAES system can operate in three states: charging phase, discharging phase and stability island mode. In the discharging phase of LAES, the turbine time constant was calculated to be 2.5 seconds. In the Cyprus system model in Figure 35, the primary response in discharging phase of LAES is considered, with the LAES time constant (Tlaes) taken to be 2.5 seconds.

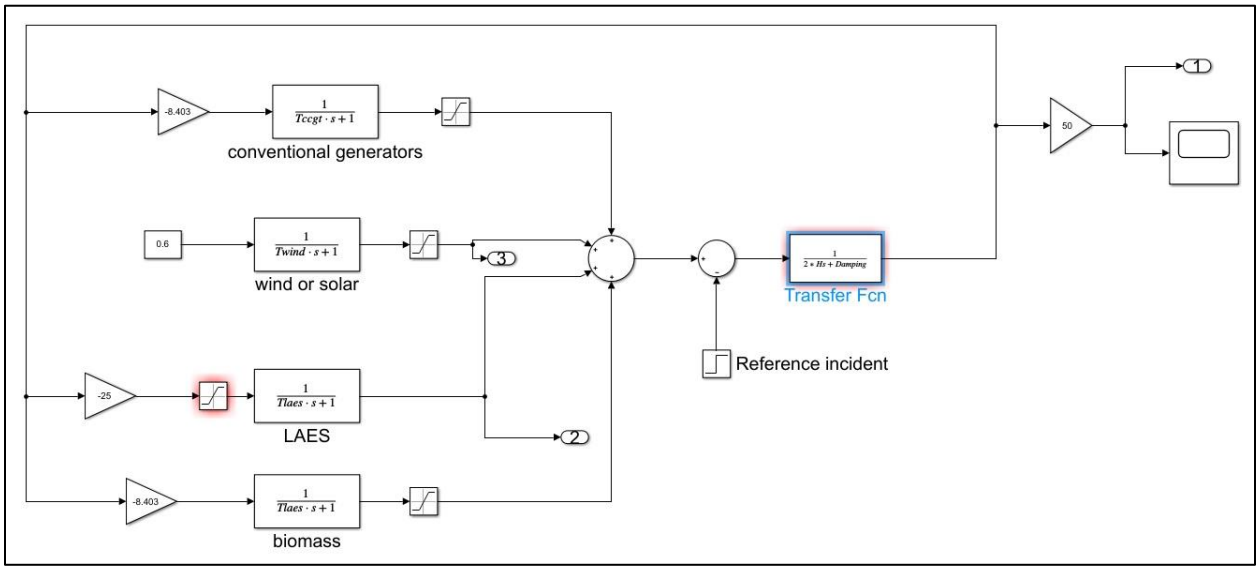

Figure 35. Basic model representative of the Cyprus system to investigate the scope of LAES to support energy storage and frequency stability requirements.

Figure 36 shows simulation results for a future scenario in which LAES is the only source of inertia in the grid. A 50 MW x 4 units of LAES capacity is considered to be installed in the grid. All the power generation is from Wind or Solar and no inertia is sourced from them. Further, it is assumed in this grid that the LAES is the largest power unit connected to the grid, that is all of the Wind and Solar generators are smaller than 50 MW. This means that the maximum possible single source of fault (reference fault) would be disconnection of one LAES unit.

In addition to the inertia from the synchronous condenser part of the LAES, LAES inertia can be further augmented by connecting flywheels in a wide range of sizes. So, in this simulation, the Flywheel size is imagined to be increased such that the inertia increases from 3 s to 6 s. For this situation, it is seen that the RoCoF varies from -1.01 Hz/s to -0.52 Hz/s and the frequency deviation varies from -2.51 Hz to -1.39 Hz. Also, for the inertia of 5.5 s, the RoCoF is -0.57 Hz/s and frequency deviation is -1.5 Hz.

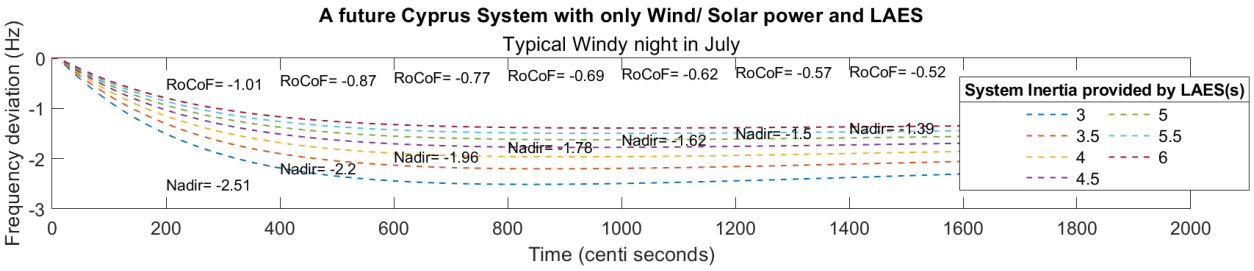

Figure 36. Simulating a future Cyprus system scenario with only Wind/ Solar power and LAES

In the next simulation, whose results are seen in Figure 37 and 38, instead of the inertia from flywheels, the capacity of the synchronous condenser part of the LAES is increased such that it can maintain the same frequency deviation (-1.5 Hz) as if the inertia is 5.5 s.

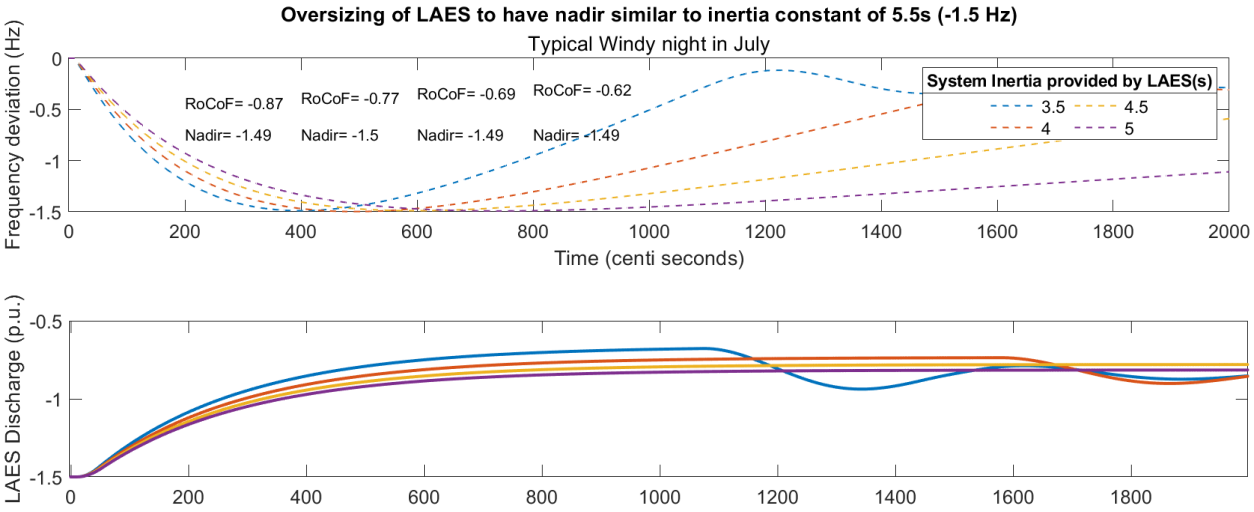

Figure 37. Increasing LAES capacity, for different inertia levels, to be able to maintain frequency deviation at the same level as if inertia is 5.5 s

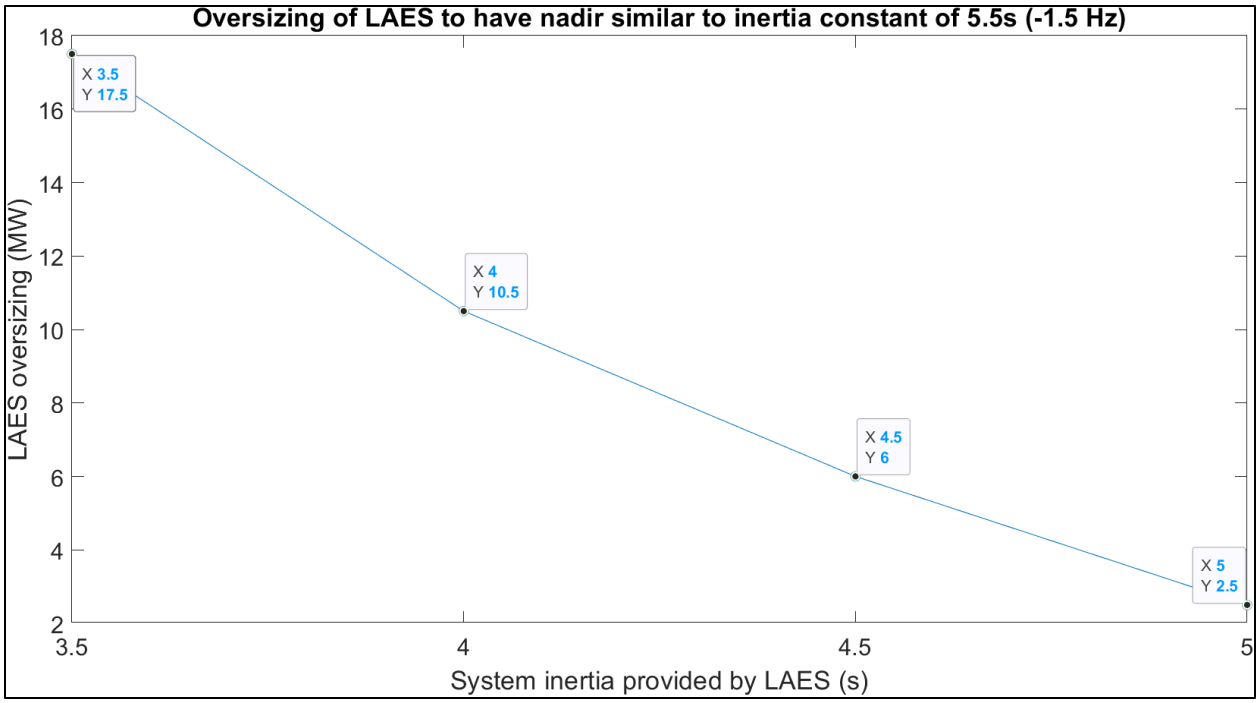

Figure 38. LAES oversizing needed for different levels of the inertia being provided by the flywheels connected to the LAES – the combination of LAES oversizing and System inertia together have a frequency nadir same as the inertia constant of 5.5 s, that is -1.5 Hz.

In Figure 38, we see that if the flywheels provide a system inertia of 4.5 s, the LAES needs to be oversized by 6 MW to have a frequency nadir same as at the inertia constant of 5.5 s (-1.5 Hz). If the system inertia value drops to 3.5 s, the LAES needs to be oversized by 17.5 MW.

6. DISCUSSION AND CONCLUSIONS

Using power system frequency response simulations, understanding was developed regarding the different factors that influence the capacity of fast ESS and inverter capacity needed to compensate for the reduction in synchronous RI. The effect of the VSG response time (VI delay) and the reference fault size on the required fast ESS capacity was noted. For the Nordic power system, simulation results compared the FFR response with different levels of KE reserve in the power grid. For the Cyprus power system, exploratory analysis looked possible LAES scope and capacity to support a 100% renewable grid.

Decline in synchronous rotational inertia is a phenomenon that future power systems must contend with. The present study highlights, that the nature and extent of this challenge is different for different power systems. Thus, the suitability of alternative solutions for low inertia depends on the system specific frequency stability criteria and requirements. For example, in the present Nordic grid, the FFR capacity of 62.4 MW suffices to improve the frequency nadir which would otherwise require almost 9.44 GWs of additional KE reserves. With the Fingrid's procurement of FFR capacity in the hourly market, this opens the opportunity for diverse possible FFR solutions to participate in the market.

On the other hand, power systems that require active inertia capacity on a more frequent basis could consider long term contracts over hourly markets to have assured inertia capacity. The relative competitiveness of inertia solutions will be different in this market.

From the simulations, it is observed that the required VI capacity increases as the VSG response time increases (higher VI delay) and, also with increases in the reference fault size. Alternatively, it may be said that the VI competitiveness decreases as VSG response time and reference fault size increases.

The required VI capacity also varies depending on the level of existing system inertia. As the system inertia declines, the rate of increase in VI capacity increases steadily and as the inertia drops to very low values, VI capacity rises much more rapidly. This is also noted in the Nordic power system where the system inertia is at a high level and relatively small FFR capacity is suitable to sustain frequency nadir above desired limits.

In other words, we observe that systems with high inertia do not have significant RoCoF dynamics and VI solutions are able to provide the required frequency nadir support. Whereas, as system inertia declines and RoCoF dynamics becomes more prominent, VI solutions are less competitive because of their higher response times compared to synchronous RI. Table 7 (see Chapter 3) underscores this observation, where different grids are noted to have either RoCoF or Nadir criteria to set the minimum inertia level in the grid.

This work was motivated by the need to understand the scope and role of LAES and other such sources of synchronous RI in supporting low inertia systems. Sources of synchronous RI such as LAES are believed to have a role in maintaining a minimum inertia base in the grid such that the RoCoF dynamics doesn't become prominent. And in this situation where there is no significant RoCoF dynamics, other inertia alternatives can competitively mitigate the occasional dips in inertia such that frequency nadir of the system is maintained above a desired limit.

This study contributes towards a long-term view of the required VI, in terms of fast energy storage capacity and inverter capacity that is required to replace the decline in synchronous RI. If high amounts of RI are maintained in the system, then further gaps in inertia requirements can be addressed with limited capacity of fast energy storage.

Thus, the initial research questions and objectives were answered as follows:

- How to approach the choice between the real and virtual inertia? What are their relative technical/ commercial competences?
    - One approach taken in this work is visualised in Figure 8, explained in Section 1.4. Overall, the Chapter 3, 4 and 5 offer a deeper and richer context into the choice between real and virtual inertia.
- What is the role of (or minimum requirement) of real inertia in the future grid?
    - The minimum inertia requirement for different power grids is explained by way of Table 6 in the Chapter 3, Literature Review.

A. For different level of grid inertia, what is the equivalent fast response capacity required to provide an inertia response that is like rotational inertia response?

a. Simulations presented in Chapter 4 address this research question.

B. Understand the different virtual inertia topologies and model a representative virtual inertia solution.
   a. This research question is addressed in a limited way in Chapter 3, and in selection of the VI model for modeling, given by Equation 11.

C. Understand, using models, the role of Liquid Air Energy Storage, as a source of rotational inertia to the grid.
   a. This is undertaken in Section 5.2, in the exploratory analysis of the Cyprus power grid.

D. Comprehend the results in specific grid scenarios.
   a. This is undertaken in Chapter 5 for the Nordic power and the Cyprus power system.

7. FURTHER RESEARCH SCOPE

More study is needed about the J_{VI} parameter as well as other parameters in the implemented VI model, and their relationship with inverter capacity sizing. Study could also be undertaken to evolve a more holistic view on solutions that combine grid reactive power as well as energy storage requirements in addition to the active power requirements. A classification of power systems may be undertaken that identifies points of transition in a power system when the RoCoF dynamics becomes more prominent than frequency nadir dynamics and inertia response time becomes more critical. The peak active-power injection was chosen as an indicator of the required fast ESS capacity – alternative approaches and designs for fast ESS capacity sizing may be explored. Also, in the present simulation for different reference fault sizes, no changes were made to the primary frequency response parameters even as the reference fault size was changed – this approach can benefit from further scrutiny and improvements as appropriate. A larger picture concerning this study is regarding the choice of energy storage technologies in the future. In addition to technical and economic criteria, choice of storages may also be driven by sustainability criteria, which could be probed further.

Also, when there is a significant demand responding to changes in frequency, for example because of greater digitalisation and electrification, the concept of Under Frequency Load Shedding Limit that is set a particular frequency point may become more of fuzzy variable. So, the concept of "Fuzzy Under Frequency Load Shedding" could be further explored. Presently UFLS is an important criterion in setting a limit on the minimum required grid inertia and maximum allowed frequency nadir.

Finally, lower inertia typically implies more inverters integrated into the grid – inverters are not majorly concerned with rapid RoCoF dynamics. Thus, points of transition in generation mix may be identified when the RoCoF dynamics becomes more of local concern around specific synchronously connected assets rather than a global concern for the entire power grid.

8. REFERENCES

[1] T. Myllyntaus, *The role of industry in the electrification of Finland*, ETLA Discussion Papers, No. 333, Helsinki, The Research Institute of the Finnish Economy (ETLA), 1990.

[2] Y. Chen, R. Hesse, D. Turschner, and H. Beck, "Improving the Grid Power Quality Using Virtual Synchronous Machines," in *International conference on power engineering, energy and electrical drives, May*, 2011, pp. 1–6.

[3] A. Monti, F. Milano, E. Bompard, and X. Guillaud, "Classical grid control: Frequency and voltage stability," in *Converter-Based Dynamics and Control of Modern Power Systems*, Academic Press, 2020, p. 33,38.

[4] T. Kerdphol, F. S. Rahman, M. Watanabe, and Y. Mitani, "Fundamental Concepts of Inertia Power Compensation and Frequency Control," in *Virtual Inertia Synthesis and Control*, Springer, 2020, p. 15,20,55.

[5] A. Fernández-Guillamón, E. Gómez-Lázaro, E. Muljadi, and Á. Molina-Garcia, "A Review of Virtual Inertia Techniques for Renewable Energy-Based Generators," in *Renewable Energy - Technologies and Applications*, IntechOpen, 2021, p. 5,6.

[6] F. Blaabjerg, Z. Chen, and S. B. Kjaer, "Power electronics as efficient interface in dispersed power generation systems," *IEEE Trans. Power Electron.*, vol. 19, no. 5, pp. 1184–1194, 2004, doi: 10.1109/TPEL.2004.833453.

[7] S. Alepuz, S. Busquets-Monge, J. Bordonau, J. Gago, D. González, and J. Balcells, "Interfacing renewable energy sources to the utility grid using a three-level inverter," *IEEE Trans. Ind. Electron.*, vol. 53, no. 5, pp. 1504–1511, 2006, doi: 10.1109/TIE.2006.882021.

[8] Central Electricity Regulatory Commission, "Indian Electricity Grid Code," no. December 2005, pp. 1–74, 2006.

[9] EPRI White Paper, "Meeting the Challenges of Declining System Inertia." Electric Power Research Institute, 2019.

[10] A. Ulbig, T. S. Borsche, and G. Andersson, “Impact of low rotational inertia on power system stability and operation,” *IFAC Proc. Vol.*, vol. 47, no. 3, pp. 7290–7297, 2014, doi: 10.3182/20140824-6-za-1003.02615.

[11] P. Tielens and D. Van Hertem, “The relevance of inertia in power systems,” *Renew. Sustain. Energy Rev.*, vol. 55, pp. 999–1009, 2016, doi: 10.1016/j.rser.2015.11.016.

[12] D. Fernández-Muñoz, J. I. Pérez-Díaz, I. Guisández, M. Chazarra, and Á. Fernández-Espina, “Fast frequency control ancillary services: An international review,” *Renew. Sustain. Energy Rev.*, vol. 120, 2020, doi: 10.1016/j.rser.2019.109662.

[13] EirGrid and SONI, “RoCoF Alternative & Complementary Solutions Project, Phase 2 Study Report,” no. March, p. 100, 2016, [Online]. Available: http://www.eirgridgroup.com/site-files/library/EirGrid/RoCoF-Alternative-Solutions-Project-Phase-2-Report-Final.pdf.

[14] V. A. V. Mohanan, I. M. Y. Mareels, R. J. Evans, and R. R. Kolluri, “Stabilising influence of a synchronous condenser in low inertia networks,” *IET Gener. Transm. Distrib.*, vol. 14, no. 17, pp. 3582–3593, 2020, doi: 10.1049/iet-gtd.2020.0178.

[15] J. H. Eto *et al.*, “Research Roadmap on Grid-Forming Inverters,” *National Renewable Energy Laboratory*. Golden, CO, p. 60, 2020, [Online]. Available: https://www.nrel.gov/docs/fy21osti/73476.pdf.

[16] S. Hamdy, F. Moser, T. Morosuk, and G. Tsatsaronis, “Exergy-based and economic evaluation of liquefaction processes for cryogenics energy storage,” *Energies*, vol. 12, no. 3, 2019, doi: 10.3390/en12030493.

[17] C. Damak, D. Leducq, H. M. Hoang, D. Negro, and A. Delahaye, “Liquid Air Energy Storage (LAES) as a large-scale storage technology for renewable energy integration – A review of investigation studies and near perspectives of LAES,” *Int. J. Refrig.*, vol. 110, pp. 208–218, 2020, doi: 10.1016/j.ijrefrig.2019.11.009.

[18] E. Borri, A. Tafone, A. Romagnoli, and G. Comodi, “A review on liquid air energy storage: History, state of the art and recent developments,” *Renew. Sustain. Energy Rev.*, vol. 137, no. December 2020, p. 110572, 2021, doi: 10.1016/j.rser.2020.110572.

[19] P. Kundur, “Power System Stability and Control,” *Power System Stability and Control, Third Edition*. pp. 1-31-13–20, 1994, doi: 10.4324/b12113.

[20] P. Denholm, T. Mai, R. W. Kenyon, B. Kroposki, and M. O. Malley, “Inertia and the Power Grid : A Guide Without the Spin,” *Natl. Renew. Energy Lab.*, p. 48, 2020, [Online]. Available: https://www.nrel.gov/docs/fy20osti/73856.pdf.

[21] H. Karbouj, Z. H. Rather, D. Flynn, and H. W. Qazi, “Non-synchronous fast frequency reserves in renewable energy integrated power systems: A critical review,” *Int. J. Electr. Power Energy Syst.*, vol. 106, pp. 488–501, 2019, doi: 10.1016/j.ijepes.2018.09.046.

[22] H. Bevrani, T. Ise, and Y. Miura, “Virtual synchronous generators: A survey and new perspectives,” *Int. J. Electr. Power Energy Syst.*, vol. 54, pp. 244–254, 2014, doi: 10.1016/j.ijepes.2013.07.009.

[23] V. Karapanos, S. W. H. De Haan, and K. H. Zwetsloot, “Testing a Virtual Synchronous Generator in a Real Time Simulated Power System,” *Int. Conf. Power Syst. Transients*, 2011.

[24] U. Tamrakar, D. Shrestha, M. Maharjan, B. P. Bhattarai, T. M. Hansen, and R. Tonkoski, “Virtual inertia: Current trends and future directions,” *Appl. Sci.*, vol. 7, no. 7, pp. 1–29, 2017, doi: 10.3390/app7070654.

[25] A. Bera, M. Abdelmalak, S. Alzahrani, M. Benidris, and J. Mitra, “Sizing of energy storage systems for grid inertial response,” *IEEE Power Energy Soc. Gen. Meet.*, 2020, doi: 10.1109/PESGM41954.2020.9281937.

[26] European Network of Transmission System Operators for Electricity, “Inertia and Rate of Change of Frequency (RoCoF),” 2020. [Online]. Available: https://eepublicdownloads.azureedge.net/clean-documents/SOC documents/Inertia and RoCoF_v17_clean.pdf.

[27] D. Zografos, “Power System Inertia Estimation and Frequency Response Assessment,” Doctoral Thesis, Electrcal Engineering, KTH Stockholm, Sweden, 2019, [Online]. Available: http://kth.diva-portal.org/smash/get/diva2:1369967/FULLTEXT01.pdf.

[28] P. M. Anderson and M. Mirheydar, “A low-order system frequency response model,”

IEEE Trans. Power Syst., vol. 5, no. 3, pp. 720–729, 1990, doi: 10.1109/59.65898.

[29] M. L. Chan, F. Schweppe, and R. D. Dunlop, "Dynamic equivalents for average system frequency behavior following major disturbances," *IEEE Trans. Power Appar. Syst.*, vol. 4, pp. 1637–1642, 1972, doi: 10.1109/TPAS.1972.293340.

[30] G. Lalor and M. O'Malley, "Frequency control on an island power system with increasing proportions of combined cycle gas turbines," *2003 IEEE Bol. PowerTech - Conf. Proc.*, vol. 4, pp. 228–234, 2003, doi: 10.1109/PTC.2003.1304727.

[31] L. Meegahapola, "Characterisation of gas turbine dynamics during frequency excursions in power networks," *IET Gener. Transm. Distrib.*, vol. 8, no. 10, pp. 1733–1743, 2014, doi: 10.1049/iet-gtd.2013.0824.

[32] T. Kerdphol, F. S. Rahman, M. Watanabe, Y. Mitani, D. Turschner, and H. P. Beck, "Enhanced Virtual Inertia Control Based on Derivative Technique to Emulate Simultaneous Inertia and Damping Properties for Microgrid Frequency Regulation," *IEEE Access*, vol. 7, pp. 14422–14433, 2019, doi: 10.1109/ACCESS.2019.2892747.

[33] R. Eriksson, N. Modig, and K. Elkington, "Synthetic inertia versus fast frequency response: A definition," *IET Renew. Power Gener.*, vol. 12, no. 5, pp. 507–514, 2018, doi: 10.1049/iet-rpg.2017.0370.

[34] European Network of Transmission System Operators for Electricity, "Fast Frequency Reserve – Solution to the Nordic inertia challenge," 2019. [Online]. Available: https://www.statnett.no/globalassets/for-aktorer-i-kraftsystemet/utvikling-av-kraftsystemet/nordisk-frekvensstabilitet/ffr-stakeholder-report_13122019.pdf.

[35] M. Kuivaniemi, N. Modig, and R. Eriksson, "Real-time estimation of frequency stability using a dynamic model tuned based on real events." CIGRE Session 48, Paris, 2020.

[36] "Cyprus Power Grid Information," 2019. https://www.iene.eu/articlefiles/chrisoxoos cyprus 19.pdf (accessed Sep. 15, 2021).

[37] "Proportion of renewable energy in Cyprus Power Grid." https://tsoc.org.cy/electrical-system/energy-generation-records/res-penetration/ (accessed Sep. 15, 2021).